Bull Volcanol (2015) 77: 14
DOI 10.1007/s00445-014-0895-6

RESEARCH ARTICLE

The 1732 Surtseyan eruption of Eggøya, Jan Mayen, North Atlantic: deposits, distribution, chemistry and chronology

Eirik Gjerløw · Armann Höskuldsson · Rolf-Birger Pedersen

Received: 28 May 2014 / Accepted: 15 December 2014 / Published online: 3 February 2015

Abstract The island of Jan Mayen in the North Atlantic Ocean is home to the world's northernmost active subaerial volcano, Beerenberg. Of the five known historical eruptions on the island, the locations of two eruptions (1732 and 1818) have not been accurately located. It is known that the 1732 and 1818 eruptions occurred on the south flank of Beerenberg, and several eruption sites have been proposed for these events. Here we show that the tuff cone of Eggøya on the SW flank of Beerenberg was the site of the 1732 eruption, based on interpretation of the deposits, field relations and historical sources. We further describe the deposits from the eruption and show that Eggøya is the largest explosive eruption described from Jan Mayen, emplacing at least at least 0.3–0.4 km^3 (VEI 4) of basanitic tephra up to distances of at least 111 km from Jan Mayen and covering a minimum area of around 500 km^2 within the 2-cm isopach. We also present our eruption scenario and show that this was an emergent Surtseyan eruption with activity shifting between tephra jetting, continuous uprush and more magmatic phases.

Keywords Surtseyan eruptions · Volcanic hazards · Jan Mayen · Tephra

Editorial responsibility: P-S Ross

Electronic supplementary material The online version of this article (doi:10.1007/s00445-014-0895-6) contains supplementary material, which is available to authorized users.

E. Gjerløw (✉) · R.-B. Pedersen
Centre for Geobiology, University of Bergen, Allegaten 41, 5007 Bergen, Norway
e-mail: eirik.gjerlow@geo.uib.no

E. Gjerløw · A. Höskuldsson
Nordic Volcanological Center, University of Iceland, Sturlugata 7, 101 Reykjavik, Iceland

A. Höskuldsson
Faculty of Earth Sciences, University of Iceland, Sturlugata 7, 101 Reykjavík, Iceland

R.-B. Pedersen
Department of Earth Science, University of Bergen, Allegaten 41, 5007 Bergen, Norway

Introduction

The eruptions of monogenetic tuff cones emerging from standing water (sea water, lakes etc.) are called Surtseyan eruptions after the Surtsey (Iceland) eruption of 1963–1967. The Surtsey eruption showed how the interaction between magma and water affected the eruption style of otherwise effusive or mildly explosive eruptions (Thorarinsson et al. 1964; White and Houghton 2000). Tephra sheets from these eruptions are characterised by rapidly thinning deposits, limited dispersal and a high proportion of fine material (Walker 1973; Cas and Wright 1987; Pyle 1989). Tuff cones and rings are both formed as a result of the magma–water interaction typical for Surtseyan and other hydromagmatic eruptions, and the morphology of the resulting landform depends on the depositional processes operating during the eruption.

Several studies have described the evolution and growth of Surtseyan edifices through lithofacies descriptions and depositional processes, but only a few such studies detail the tephra sheets of such eruptions (e.g. Matsson and Höskuldsson 2011). Tuff cones like the ones at Surtsey (Thorarinsson et al. 1964), Capelinhos (Cole et al. 2001), São Roque (Zanon et al. 2009), Ilchulbong (Sohn and Chough 1992) and Capelas (Solgevik et al. 2007; Mattsson 2010) have higher aspect ratios (height/crater diameter), a steep cone morphology and are dominated by fallout deposits (Wohletz and Sheridan 1983; Sohn 1996), while tuff rings like the ones at Hverfjall

(Matsson and Höskuldsson 2011) and Karmskoye lake (Belousov and Belousova 2001) have low angle ring morphology, low aspect ratios and are dominated by base-surge deposits (Sohn 1996; Vespermann and Schmincke 2000; Solgevik et al. 2007). Tephra formed by Surtseyan volcanism is generally characterised by having a blocky morphology, low vesicularity and a fine grain size as a result of hydromagmatic fragmentation (Dellino et al. 2001).

Well described observed examples of Surtseyan volcanism include the 1963–1967 Surtsey Island eruption in Iceland (Thorarinsson et al. 1964) and the 1957–1958 Capelinhos eruption in the Azores (Cole et al. 2001). The main primary hazards of these eruptions were tephra fall, which in Capelinhos and Surtsey reached distances exceeding 20 km, pyroclastic surges that reached distances of at least 2 km and ballistic bombs within 2 km of the vents.

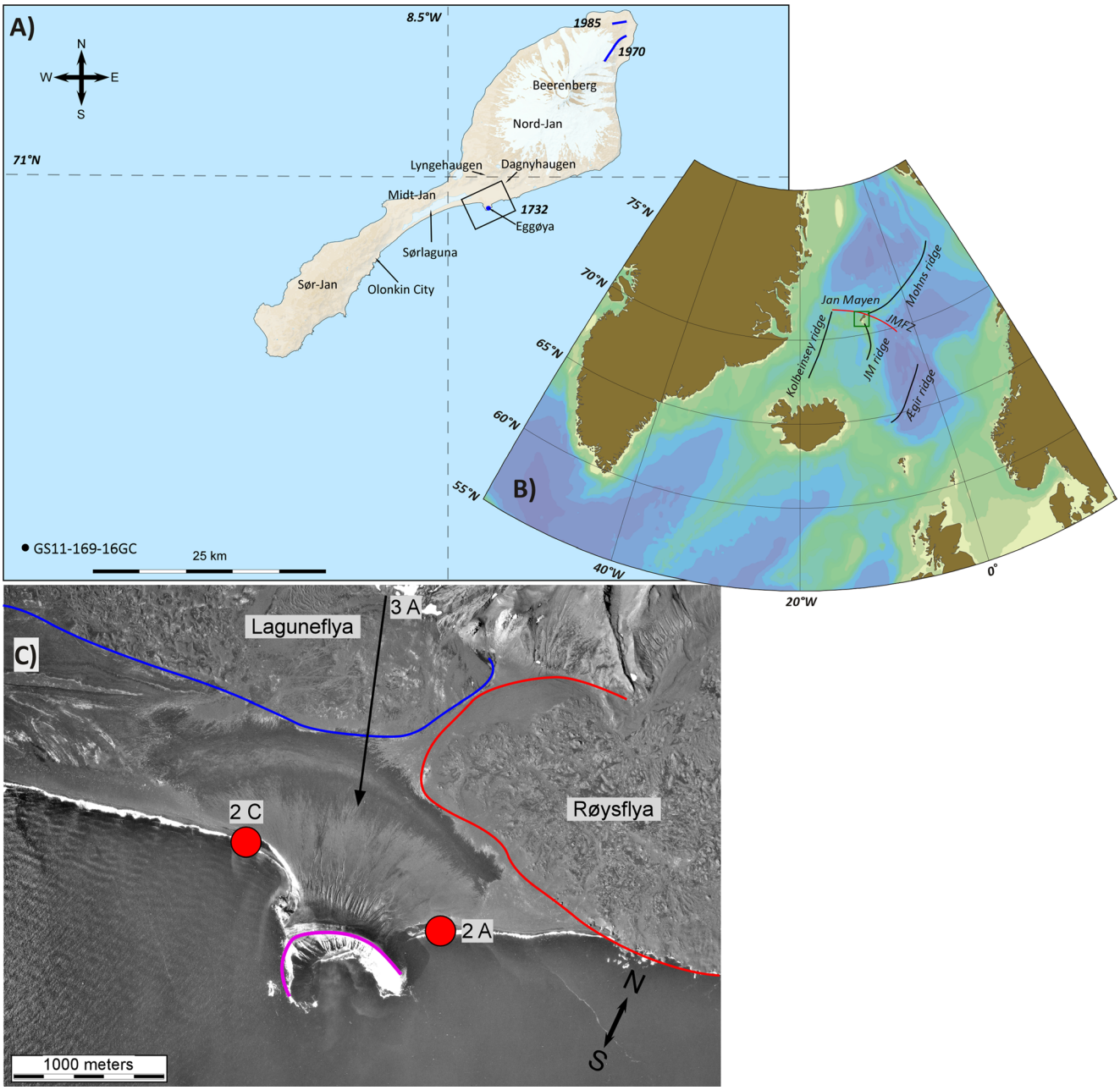

Fig. 1 **a** Map of Jan Mayen showing eruption locations. All major geographical locations mentioned in the text are indicated on the map, including the position of core GS11-169-16GC in the southwest corner of the map. Base map used with permission, © Norsk Polarinstitutt. **b** Regional map showing the location of Jan Mayen, Mohns Ridge, Kolbeinsey Ridge, Ægir Ridge, Jan Mayen Ridge and the Jan Mayen Fracture Zone (JMFZ). **c** An aerial photo of Eggøya and the Røysflya and Laguneflya lava flows that were previously suggested to have been formed during the 1732 and 1818 eruptions. Section of aerial photo JM75 7279, with permission, © Norsk Polarinstitutt. *Red dots* represent picture locations for Fig. 2a and c, while the *black arrow* represents the line of sight from Fig. 3a

Numerous remains of tuff cones are present along the coasts of Jan Mayen, a volcanic island in the North Atlantic Ocean, but no explosive activity from Jan Mayen has previously been described in detail. Jan Mayen is located between Norway, Greenland and Iceland (Fig. 1), making it the northernmost active subaerial volcano in the world. The volcanic history of the island is little known, though the island was first discovered in the fifteenth century and the first reliable description of volcanic activity dates from 1732 when an eruption was witnessed by a group of German whalers (Anderson 1746). Contemporary descriptions of this eruption mention ash clouds, deposition of ash around 111 km from the island and a thick layer of ash covering parts of Jan Mayen. Stemming back to Wordie (1922), this eruption has been attributed to craters north of Eggøya: 'It is a further confirmation that the three possible places for such an outburst are all near the foot of the mountain on the south side, namely Berna crater, Egg Bluff (Eggøya), and a subsidiary crater beside Vogt crater. I regard the latter as the likeliest locality despite hot steam still coming from Egg Bluff'.

William Scoresby Jr. witnessed an eruption in 1818 (Scoresby 1820) and observed 'considerable jets of smoke discharged from the earth every 3–4 minutes'; he also mentions that another ship witnessed a reddish glow in the sky in the same area around the same time. Changes in the coastline between old maps indicate at least one more eruption between 1650 and 1882 (Sylvester 1975), forming a coastal lava plateau in the north east tip of the island. In recent times, more effusive eruptions occurred in 1970 (Siggerud 1972) and 1985 (Imsland 1986) on the north east tip of the island extending the coastal lava plateaus.

In this paper, we provide a general study of the 1732 AD Surtseyan eruption of Jan Mayen. We use field observations and historical sources to show that the source of this first eruption observed on the island was Mount Eggøya, a Surtseyan tuff cone, and that it took place in spring 1732 AD, thus showing that the crater, Dagnyhaugen, which was previously suggested as the site for this eruption (Wordie 1926), is somewhat older. Further, we use the tephra deposits, their chemistry, distribution, grain size variations and morphology to estimate volume and mass produced, and to give insights into the eruption chronology and eruption styles of Eggøya.

Geological setting and eruptions

Geological setting

Jan Mayen (71°N, 8°W) is located at the northern end of the Jan Mayen ridge and south of the intersection between Mohns ridge and the Jan Mayen Fracture Zone (JMFZ). The JMFZ displaces the Mid Atlantic ridge from the Kolbeinsey ridge in the south to Mohns ridge in the north by some 200 km (Fig. 1b). It has been suggested that the origin of the volcanism on Jan Mayen is related to heat from Mohns ridge penetrating through the JMFZ and into the Jan Mayen ridge continental fragment (Haase et al. 1996). Trønnes et al. (1999) suggested that the volcanic rocks of Jan Mayen originate predominantly from low degree melting of an enriched mantle source.

The volcanism on Jan Mayen lines up along a north-east trending system of fissures and craters, with two main eruptive centres: the stratovolcano of Beerenberg, which reaches an altitude of 2277 m above sea level, situated on Nord-Jan (the northern part of the island); and a volcanic ridge/plateau consisting of numerous fissures, craters and domes on Sør-Jan (the southern part of the island) (Fig. 1a). On Nord-Jan, eruptions have occurred at the central crater on the stratovolcano Beerenberg, on short radial fissures or single craters on its flanks and along the periphery of the volcano, while on Sør-Jan the eruptions have occurred on short north-east trending fissures, single craters and domes (Imsland 1978). Numerous remains of tuff cones are evident along the coastline on Midt-Jan (the central isthmus connecting the north and south parts) attesting to shallow submarine to emergent eruptions. Further, palagonite tuffs of probable sub-glacial origin are found along the coast of Nord- and Midt-Jan (Hawkins and Roberts 1972).

Jan Mayen Island consists of alkaline volcanic rocks, ranging from primitive ankaramites to evolved trachytes (Imsland 1984). The ankaramites were erupted on the peripheral flanks of Beerenberg, ankaramitic basalts on Nord- and Midt-Jan, basaltic tristanites (porphyritic and aphyric) found on Sør-, Midt- and Nord-Jan, and, finally, tristanites and trachytes mainly occurring as domes and coulées on Sør-Jan with one exception on Midt-Jan, the Wildberget coulées (Imsland 1984).

The deposits of Jan Mayen were divided into five different volcano-stratigraphic units by Imsland (1978) based on and modified from the work of Carstens (1962) and Fitch (1964) as follows: (1) 'Hidden formations' that the island rests upon, extending up to present sea level; (2) Havhestberget hyaloclastite formation, produced in shallow submarine eruptions when the island was emerging from the sea; (3) Nordvestkapp subaerial formation, a pre-Holocene lava pile formed after the island had emerged; (4) Inndalen formation, a Holocene post-glacial formation consisting of lavas of basanite–tephrite to trachytic composition; and (5) glacial and coastal sediments.

All the rocks on Jan Mayen are normally magnetised and are thus younger than 700 ka (Fitch et al. 1965b; Cox 1969; Imsland 1978; Cromwell et al. 2013). Exposed Jan Mayen rocks dated by Cromwell et al. (2013) show Ar/Ar ages ranging from present day back to 460.9±55.8 ka.

Holocene volcanism on Sør-Jan has produced effusive lavas, scoria cones, domes and coulées. The isthmus Midt-

Jan is characterised by scoria cones and tuff cones formed by shallow marine to emergent explosive Surtseyan eruptions. On Nord-Jan, eruptions have been mainly in the form of effusive lava and scoria cones forming flank eruptions and explosive phreatomagmatic eruptions at the summit (Fitch 1964; Imsland 1978). One eruption originated from the Eggøya crater, a horseshoe shaped crater located at sea level on the SW flank of Beerenberg (Fig. 1); the crater rim reaches an altitude of 215 m with a rim diameter of 500–600 m (Fig. 1c).

Holocene and historical eruptions

The recurrence rate for Jan Mayen eruptions was estimated by Imsland (1978) to be 100–133 years, based on counting the number of Holocene monogenetic vents; this estimate excludes all summit eruptions of Beerenberg and any vents covered by present day glaciers. In historical times, however, the recorded eruptions have been one to two per century. Four historical eruptions are mentioned on the island (1732, 1818, 1970 and 1985); one additional eruption was suggested by Sylvester (1975) to have occurred between 1650 and 1882. Of these, only the 1970 (Siggerud 1972) and 1985 (Imsland 1986) flank eruptions are well known and described to some extent. The suggestion of an eruption between 1650 and 1882 is based on changes to the coastline observed between maps from 1650 (Blaeu 1650) and 1882 (Boldva 1886). In the map from 1882, a new patch of land (Kokssletta) was mapped on the NE tip of the island, indicating that an eruption had occurred during the aforementioned time period (Sylvester 1975). The 1818 eruption was observed by William Scoresby Jr. when he was passing the island in April of the same year (Scoresby 1820). This eruption was also witnessed by Captain Gilyott of Richard of Hull (Barr 2003).

During the spring of 1732, an eruption was reported on Jan Mayen. It was observed on the 17th of May by Jacob Jacobsen Laab, the Captain of a German whaling ship lying becalmed around 22.2 km (3 German miles) south of Beerenberg. He and his crew noted an explosive outburst taking place at the foot of Beerenberg. They described 'flames' shooting out, followed by the formation of a dark cloud. The 'flames' were only observed on May 17th; however, the black cloud was observed during the 4 days the ship lay there waiting for favourable winds. Once the wind changed, the ship and crew could proceed with their journey. Captain Laab last mentioned the eruption when his ship was some 111 km (15 German miles) from the island, as the ship's deck and sails were covered with volcanic ash (Wordie 1922). In June of the same year, the Dutch whaling Captain Alicke Payens was ashore on Jan Mayen. He reported volcanic ash from the recent eruption with a thickness of at least 20–30 cm (Barr 2003).

Previously, the 1732 eruption had been allocated to the Dagnyhaugen crater (Scoresby 1820; Wordie 1922) on the SW flank of Beerenberg. Further, the Røysflya (Fig. 1) lava flow had been allocated to the eruption of 1732 and the Laguneflya (Fig. 1c) lava flow to the 1818 eruption (Imsland 1978). Our study shows that both lava flows are covered by the Eggøya tephra sheet and must hence be older, and that the eruption of 1732 was a shallow submarine to emergent event that formed Mount Eggøya.

Methods

Field work on Jan Mayen

Field mapping and sampling of the tephra sheet from the Eggøya eruption were conducted during the summers of 2011 and 2012 on most of Jan Mayen, with the exception of the SE coast of Sør-Jan and the NE parts of Beerenberg (Nord-Jan); these locations were excluded due to remoteness, rugged terrain and glacial cover, along with poor preservation of the tephra layer at higher altitudes. The Eggøya tuff cone was also examined, but the emphasis was placed on the tephra sheet due to the consolidated nature, steep walls and hence inaccessibility of large parts of the tuff cone. The geographic position of the island also meant that above 100 m altitude, permafrost prevailed in surface soil and sediments, thus preventing sectioning. The Eggøya tephra sheet was found at 25 locations and identified in the field based on the colour, thickness, phenocryst content and relative stratigraphic position compared to other tephra layers observed in soil profiles. At each location, the relative stratigraphic position of the tephra and phenocryst content was recorded, the thickness of the tephra sheet was measured and in proximal areas where its internal stratigraphy was prominent, it was recorded and sub-sampled.

Offshore gravity cores

Off the shore of Jan Mayen, we sampled gravity cores from 11 different locations in an attempt to better understand the eruptive history of the island (Gjerløw et al., in preparation). A cryptotephra horizon from one of these cores was sampled for this study. The core was collected at 70° 37.860′ N and 9° 44.004′ W, about 60 km southwest of Eggøya and roughly 34 km southwest of the southern tip of Jan Mayen (Fig. 1a).

Laboratory work

Grain-size analysis was carried out at the University of Iceland where the samples of Eggøya ash from 16 distal and four proximal sections were first dried and then hand sieved down to 4 φ (>63 μm) at 0.5-φ intervals. The fraction finer than 4 φ (<63 μm) was further analysed by a Micromeritics SediGraph III 5120 down to 10 φ (1 μm).

Table 1 Chemical composition of Eggøya samples

Sample	SiO_2	TiO_2	Al_2O_3	FeO	MnO	MgO	CaO	Na_2O	K_2O	P_2O_5	Total
P1-1	47.12	3.19	16.23	10.11	0.22	4.34	9.53	3.43	2.94	0.61	97.72
P1-1	48.14	3.26	16.38	10.26	0.22	4.14	9.43	3.61	3.23	0.68	99.35
P1-1	47.71	3.31	15.75	10.22	0.24	3.93	8.67	3.60	3.38	0.74	97.55
P1-1	47.99	3.27	16.11	10.57	0.21	3.94	8.65	3.63	3.19	0.69	98.25
P1-1	47.64	3.21	16.24	10.22	0.23	4.48	9.71	3.48	2.91	0.63	98.74
P1-1	48.77	3.32	16.20	10.54	0.20	4.10	8.75	3.75	3.26	0.73	99.62
P1-1	47.81	3.22	16.26	10.21	0.21	4.24	9.32	3.53	3.03	0.64	98.45
P1-1	48.58	3.15	16.20	10.87	0.22	4.33	9.26	3.55	2.99	0.65	99.78
P1-1	46.57	3.23	16.39	10.18	0.21	4.12	8.98	3.50	3.16	0.67	97.01
P1-2	47.86	3.24	16.17	10.61	0.23	4.31	9.46	3.55	3.05	0.63	99.12
P1-2	47.36	3.27	16.51	10.34	0.23	4.28	9.44	3.63	3.11	0.65	98.82
P1-2	47.37	3.20	16.26	10.30	0.18	4.43	9.63	3.43	2.96	0.63	98.39
P1-2	47.71	3.30	16.27	10.61	0.21	4.11	9.21	3.57	3.15	0.69	98.83
P1-2	47.79	3.14	16.40	10.03	0.22	4.23	8.99	3.48	3.06	0.63	97.96
P1-2	47.82	3.14	16.42	9.77	0.19	4.40	9.06	3.42	3.08	0.63	97.94
P1-2	47.01	3.23	16.45	10.41	0.22	4.42	9.34	3.57	2.92	0.66	98.25
P1-2	46.77	3.30	16.08	10.83	0.21	4.02	9.27	3.54	3.13	0.66	97.81
P1-2	47.74	3.24	16.54	10.14	0.23	4.48	9.49	3.39	3.13	0.64	99.02
P1-3	48.21	3.22	16.19	9.96	0.22	4.35	9.06	3.53	3.01	0.66	98.40
P1-3	47.10	3.24	16.39	9.60	0.20	4.25	9.62	3.45	2.92	0.65	97.43
P1-3	47.43	3.16	16.53	9.92	0.24	4.19	9.17	3.57	3.10	0.64	97.94
P1-3	47.65	3.34	16.02	10.41	0.22	4.04	9.40	3.56	3.09	0.67	98.41
P1-3	47.46	3.24	16.64	10.34	0.19	4.26	9.38	3.51	2.94	0.65	98.61
P1-3	48.42	3.24	16.28	10.29	0.22	4.25	9.21	3.39	2.99	0.66	98.96
P1-3	47.36	3.22	16.47	10.11	0.24	4.21	9.21	3.59	3.07	0.62	98.09
P1-3	47.53	3.29	16.23	10.14	0.23	4.46	9.46	3.50	3.03	0.64	98.50
P1-3	46.49	3.33	15.93	11.08	0.24	4.23	9.43	3.67	3.08	0.67	98.16
P1-4	46.23	3.21	16.22	10.35	0.22	4.52	9.68	3.66	2.88	0.67	97.65
P1-4	47.29	3.29	16.00	10.04	0.24	4.07	9.04	3.55	3.18	0.68	97.37
P1-4	47.99	3.16	16.36	10.28	0.21	3.88	8.58	3.61	3.42	0.64	98.12
P1-4	47.52	3.25	16.07	10.58	0.20	4.27	9.24	3.61	3.10	0.66	98.50
P1-4	46.62	3.26	16.18	10.08	0.22	4.35	9.63	3.52	3.06	0.68	97.61
P1-4	47.41	3.24	16.31	10.60	0.23	4.39	9.47	3.40	2.97	0.65	98.66
P1-4	47.38	3.26	16.38	10.40	0.19	4.19	9.09	3.75	3.19	0.67	98.50
P1-4	48.76	3.22	16.15	10.53	0.22	3.89	8.46	3.77	3.54	0.67	99.22
P1-4	46.49	3.37	16.15	10.26	0.21	3.99	8.78	3.54	3.17	0.71	96.68
P1-4	47.19	3.28	15.73	10.19	0.23	4.35	9.56	3.49	2.96	0.64	97.60
P1-5	48.01	3.26	16.33	10.52	0.21	4.33	9.76	3.47	2.97	0.69	99.55
P1-5	47.67	3.24	16.11	10.29	0.22	4.01	8.64	3.76	3.22	0.70	97.86
P1-5	48.46	3.33	16.20	10.21	0.18	4.11	9.18	3.54	3.31	0.69	99.20
P1-5	47.33	3.25	16.15	10.73	0.23	4.25	9.19	3.46	2.98	0.68	98.24
P1-5	47.17	3.20	16.06	10.88	0.22	4.35	9.43	3.62	3.04	0.66	98.63
P1-5	47.18	3.22	16.02	10.77	0.20	4.43	9.63	3.44	2.96	0.64	98.49
P1-5	46.93	3.25	16.12	10.26	0.22	4.40	9.48	3.42	2.98	0.69	97.75
P1-5	46.54	3.23	15.92	10.90	0.23	4.43	9.23	3.44	3.04	0.68	97.64
P1-6	46.54	3.23	15.92	10.90	0.23	4.43	9.23	3.44	3.04	0.68	97.64
P1-6	47.47	3.22	16.12	9.90	0.22	4.44	9.39	3.36	2.85	0.68	97.65
P1-6	47.27	3.25	16.34	10.48	0.23	4.38	9.67	3.45	3.12	0.67	98.84
P1-6	47.28	3.20	16.53	10.12	0.23	4.35	9.64	3.50	2.98	0.66	98.50

Samples from the core were prepared by drying 0.5-cm slices of sediment and weighing them before wet sieving. The concentration of tephra in the sample was determined by counting the number of tephra grains by microscope. Results were then scaled to the dry weight of the sample. Tephra grains collected from the gravity core, ranging from 3 φ (125 μm) to 0 φ (1000 μm), were used for electron microprobe analysis along with tephra shards in the size range of 2.5–2 φ (180–250 μm) from sections T1, P11, E1, E2, SE, SW1 and NW1 (Tables 1 and 2), and all the samples in the P1 section were analysed in an electron microprobe. All samples were mounted in epoxy, polished and carbon coated prior to analysis by electron microprobe for major elements. The glass from these deposits is microcrystalline and, as a result, areas with low concentrations of microlites were targeted for analysis. The major element chemistry was analysed with a Cameca SX100 electron microprobe at the School of Geosciences, University of Edinburgh, using the settings

Table 1 (continued)

Sample	SiO_2	TiO_2	Al_2O_3	FeO	MnO	MgO	CaO	Na_2O	K_2O	P_2O_5	Total
P1-6	47.61	3.22	16.15	10.02	0.20	4.24	9.43	3.70	2.97	0.63	98.16
P1-6	47.22	3.22	16.16	10.42	0.22	4.39	9.61	3.38	2.90	0.67	98.17
P1-6	47.15	3.21	16.49	10.21	0.23	4.41	9.34	3.50	2.98	0.63	98.15
P1-6	47.44	3.23	16.18	10.07	0.22	4.37	9.46	3.56	3.11	0.66	98.31
P1-6	47.88	3.20	16.47	10.21	0.21	4.37	9.54	3.54	3.00	0.66	99.08
P1-6	48.28	3.24	16.22	10.40	0.22	4.31	9.62	3.66	3.02	0.66	99.62
SW1	48.17	3.26	16.33	10.46	0.22	4.34	9.29	3.53	3.16	0.67	99.43
SW1	47.40	3.25	16.06	10.26	0.21	4.16	9.31	3.67	3.28	0.66	98.28
SW1	47.83	3.23	16.22	10.40	0.21	4.42	9.88	3.36	3.00	0.65	99.21
SW1	47.44	3.34	15.92	10.41	0.23	4.39	9.50	3.30	3.00	0.67	98.21
SW1	46.81	3.24	16.28	10.36	0.19	4.28	9.56	3.44	2.89	0.63	97.68
SW1	48.14	3.26	16.03	9.75	0.20	3.86	8.96	3.87	3.36	0.71	98.15
SW1	47.62	3.23	15.97	9.87	0.22	4.38	9.46	3.48	3.04	0.68	97.97
SW1	47.69	3.21	16.23	10.13	0.22	4.41	9.42	3.62	3.00	0.64	98.56
SW1	47.88	3.24	16.03	10.31	0.22	3.95	8.74	3.83	3.34	0.70	98.26
SE	47.92	3.25	16.32	10.43	0.23	4.33	9.11	3.59	3.16	0.67	99.02
SE	46.71	3.27	16.31	10.23	0.21	4.31	9.37	3.46	3.08	0.66	97.62
SE	47.28	3.21	16.27	10.60	0.19	4.43	9.55	3.22	2.97	0.66	98.38
SE	47.25	3.27	16.20	10.45	0.21	4.46	9.36	3.56	2.99	0.68	98.42
SE	47.54	3.16	16.67	10.23	0.20	4.31	9.65	3.40	2.90	0.66	98.73
SE	47.58	3.17	16.52	10.47	0.23	4.15	9.11	3.57	3.10	0.68	98.57
SE	47.43	3.33	16.40	10.82	0.20	4.29	9.18	3.52	3.06	0.71	98.94
SE	47.03	3.20	16.45	10.32	0.22	4.31	9.28	3.46	2.92	0.68	97.88
P11	48.13	3.24	16.05	9.92	0.22	4.10	8.77	3.59	3.20	0.71	97.93
P11	48.35	3.25	16.19	10.86	0.23	4.32	9.12	3.42	3.03	0.71	99.47
P11	47.49	3.25	16.53	10.46	0.23	4.11	9.44	3.48	2.94	0.69	98.63
P11	47.68	3.23	16.24	10.30	0.21	4.43	9.45	3.46	2.89	0.71	98.61
P11	47.75	3.20	16.12	9.94	0.22	4.44	9.50	3.46	2.91	0.66	98.20
NW1	47.53	3.32	15.81	10.60	0.21	4.22	9.09	3.57	3.20	0.72	98.27
NW1	48.18	3.20	16.55	10.23	0.22	4.41	9.50	3.48	3.01	0.65	99.43
NW1	47.74	3.29	16.21	10.67	0.23	4.37	9.47	3.58	3.15	0.68	99.38
NW1	47.07	3.29	15.63	10.98	0.19	4.25	9.18	3.52	3.04	0.67	97.83
NW1	46.86	3.34	15.87	10.69	0.22	4.34	9.55	3.48	3.08	0.71	98.15
Core Eggøya	46.87	3.22	15.68	10.61	0.19	4.46	9.35	3.50	3.01	0.63	97.51
Core Eggøya	47.40	3.25	16.06	10.52	0.19	4.47	9.77	3.40	2.95	0.63	98.65
Core Eggøya	47.84	3.27	15.94	10.33	0.22	4.14	9.14	3.61	3.13	0.68	98.30
Core Eggøya	47.84	3.26	15.47	10.55	0.23	4.48	9.64	3.34	2.99	0.65	98.44
Core Eggøya	47.56	3.23	16.08	10.51	0.22	4.23	9.55	3.30	3.11	0.65	98.45

Table 2 Soil section information

Section	Total depth (cm)	EØ thickness	Cover above EØ	Soil under EØ	Total soil thickness	Number of other layers	Notes
SW1	50	4	5	3	8	0	Bottom is beach sand
SW2	17	3	6	8	14	0	
SW3	11	1.5	4	5.5	9.5	0	
SW4	17.5	2.5	6	9	15	0	
SW5	23	2	7	14	21	0	
SW6	10	1	4	5	9	0	
SW7	10.5	2.5	5	3	8	0	
SW8	42	1	5	36	41	0	
SE	20	8	6	6	12	0	
P1	240	240	0	0	0	0	
P2	110	48	0	0	0	0	Top reworked
P3	87	37	0	0	0	0	Top 50 cm reworked
P4	97	60	0	30	30	1	Top 8 cm reworked
P5	112	107	0	5	5	0	
P6	59	59	0	0	0	0	
P7	166	160	0	6	6	0	
P8	100	100	0	0	0	0	
P9	87	87	0	0	0	0	
P10	87	66	0	20	20	0	Top 1 cm reworked
P11	270	10	5	8	173	14	
NW 1	56	13	10	7	37	2	
NW 2	10	2.5	7.5	0	7.5	0	
NW 3	32.5	10.5	0	0	0	0	22 cm reworked ash on top
NW 4	15	10	5	x	x	0	x=not measured
NW 5	40	10	0	0	0	0	30 cm reworked

described by Hayward (2012) to minimise sodium loss. Grain morphology was studied at the University of Iceland using a Hitachi Model TM3000 Tabletop scanning electron microscope (SEM) and at the University of Bergen using a Zeiss Supra 55 VP scanning electron microscope. For imaging, grains in the range of 3–4 φ (125–63 μm) were used and gold coated prior to analysis. For stereomicroscopic analysis, particles between 1.5 and 1 φ (500–355 μm) and 2.5–2 φ (250–180 μm) were used. The density of the tephra was measured by using a standard pycnometer flask, and the bulk density of the deposit was calculated by weighing dried samples of known volume.

Calculations

An isopach map of the tephra layer was compiled using a triangular method between the 25 soil sections measurements during the field seasons in 2011 and 2012. Volumes of the tephra deposit were calculated using the empirical integrations of Bonadonna and Costa (2012) (Weibull), Bonadonna and Houghton (2005) (power law), Fierstein and Nathenson (1992) (two and three exponential line segments), and the inversion technique of Connor and Connor (2006).

The total grain size distribution for the whole deposit was calculated using the Matlab script TOTGS of Biass and Bonadonna (2014) for running the Voronoi tessellation method of Bonadonna and Houghton (2005).

Degree of sorting and the Inman sorting coefficient (σφ) was calculated for individual samples using the gradistat version 8 spreadsheet for Excel (Blott and Pye 2001).

Results

Eggøya tuff cone

The Eggøya tuff cone is partly eroded, with approximately 40 % of the original area remaining. The north flank of Eggøya is relatively intact and has only been affected by wind erosion. This sector of Eggøya has a radius from the centre of the crater ranging from 1 to 1.5 km. The northeast part of the tuff cone displays inward slumping and slumping parallel to

the coast (Fig. 2a). The SE part of Eggøya, which is the part of the tuff cone that is most exposed to the sea, has been subjected to extensive marine and wind erosion, causing the partial opening of the cone towards the sea (Fig. 1a). Large blocks have broken off from the tuff cone following large earthquakes in 1935 (King and Jennings 1939). The aspect ratio, i.e. rim height/rim diameter, of Eggøya is 0.33, similar to tuff cones in Hawaii and Iceland (Wohletz and Sheridan 1983).

The remaining parts of the crater surrounding the vent consist of consolidated tuff, with cracks still venting warm air and steam (Siggerud 1972). Old maps and drawings (Mohn and Wille 1877; Boldva 1886) show that most of the erosion appears to have happened within the first 100–150 years after the eruption. The present-day coastline has been extended by up to 1.5 km compared to pre-eruption conditions.

The deposits in the exposed external flanks of the tuff cone are thinly to thickly bedded, and bomb sags (Fig. 2b) are common. The tephra making up the tuff cone is palagonised towards the centre of the cone, and the grain size of the tuff cone deposits was not measured directly as a consequence of this. Thin-section studies of the palagonite suggests that the palagonised matrix making up most of the cone originally consisted of fine to medium ash sized particles, but lapilli size fragments are common. One sample from the flank of the cone where the deposit is not palagonised has a median grain size of 1.7 φ (355–200 μm) and is composed mainly of ash sized particles (85 wt.% of the particles are smaller than −1 φ or 2 mm). Along a 0.75-km-long section from the tuff cone centre to its flanks in the west, palagonisation decreases, layers get thinner and ballistic bombs become less common. Dunes are very prominent along the section (Fig. 2c). A section in the NE flank of the tuff cone shows inward slumping along many small faults. The faults (Fig. 2a) do not extend throughout the entire stratigraphy of the tuff cone, and most are accompanied by ductile deformation of the tephra layering.

Accidental lithic fragments and bombs are concentrated in some stratigraphic horizons, and they are commonly associated with bomb sag structures in the underlying layers. In some exposed parts of the flank, they make up between 0.5 and 2 % of the exposed area, but the concentration varies greatly laterally and is therefore hard to assess. Away from the vent, their size drops quickly but they are still prominent in the exposed flank sections of the tuff cone (up to 1 km from the vent), while in the most proximal section (P1) of the tephra sheet, some 1.8 km from the vent, lithics are indiscernible with the naked eye due to the generally fine grain size of the tephra sheet, and bomb sized fragments are absent. The lithic fragments observed within the tuff cone and in proximal sections of the tephra sheet are made up of trachyte, altered reddish basalts and unaltered basalts. Accidental lithics (xenoliths) from Eggøya were described by Tyrrell (1926) as being composed of basanite–trachybasalt, trachyandesite and trachyte.

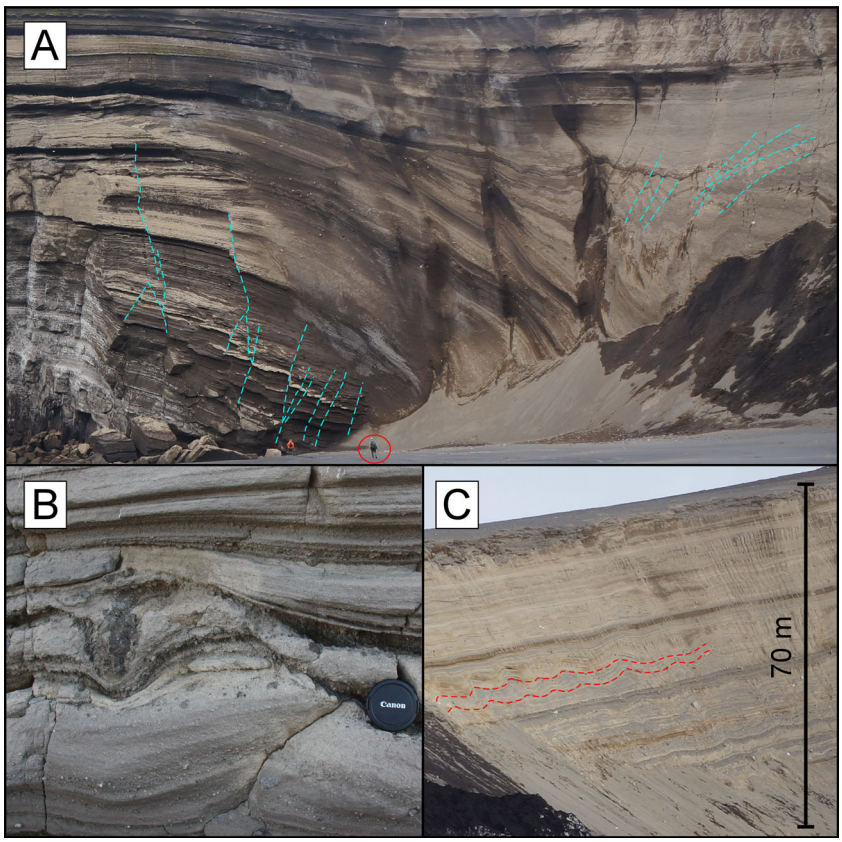

Fig. 2 Photos of the Eggøya tuff cone. **a** Northeast wall of the cone, faults and slumping marked; notice the ductile deformation in the lower parts of the cone; people in lower edge for scale. **b** Bomb sag on the crater rim, with lens cap for scale. **c** Dunes in the partly eroded SW flanks of the cone; see Fig. 1 for picture locations

The remainder of this section deals with the Eggøya tephra sheet only.

Eggøya tephra sheet

In the area closest to the tuff cone, the Eggøya tephra sheet formed surface deposits with little to no vegetation cover (Fig. 3a). It was observed to cover all of the lavas that flowed to the coast south of Beerenberg. These lavas originated from the Dagnyhaugen and Lyngehaugen craters (Fig. 1). In the proximal sections, internal layering is visible in the tephra sheet (Fig. 3b), but it disappears towards the medial and distal areas. On the Laguneflya and Røysflya lava flows, the tephra deposits formed onion-like structures in the lava field (Fig. 3c); these onion-like structures were formed where the tephra deposit was mantling an uneven surface, and subsequent erosion then exposed different stratigraphic layers on the surface forming this pattern. Occasionally, holes of up to 1–3 m in diameter occurred in this tephra layer (Fig. 3d). The cavities formed due to the melting of snow underneath the tephra and the collapse of the tephra into these cavities. In more distal areas, the tephra formed a single layer without any apparent internal structure. The Eggøya tephra sheet is the most widely distributed tephra layer we found on Jan Mayen. Due to permafrost, it was mostly observed at lower altitudes and in the coastal areas. Only in two places could we observe the primary tephra layer at an altitude as high as 100 m. In 25 sections, we observed the Eggøya tephra sheet as the shallowest tephra layer. Its thickness ranges from around 2.1 m closer to Eggøya down to 1–2 cm in the SW parts of Jan Mayen, while the tuff cone has a maximum thickness of more than 215 m.

Proximal sections

In the proximal areas of Røysflya and Laguneflya (Fig. 1), the Eggøya tephra sheet remains free of vegetation and soil and, in some locations, it is underlain by a thin layer of moss and soil covering the lava flows upon which it was deposited. In these areas, thermokarst depressions occur quite commonly, where the tephra deposit has collapsed into underlying cavities (Fig. 3d).

The most proximal section of the tephra sheet (P1; Fig. 4a) with a total thickness exceeding 210 cm is described below using the nomenclature in Sohn and Chough (1989). It contains five distinct units.

Unit 1 starts with a medium bed (25 cm) of coarse layered ash with some internal laminae, followed by a medium bed (17.5 cm) of medium to coarse ash with accretionary lapilli (ACL) up to 0.5 cm in size (sample P1-1 from this layer); the ACL disappear towards the top of this layer. The top of this unit consists of a thin bed (8 cm) of coarse ash grading first to medium ash and then to fine ash; all of these contain ACL.

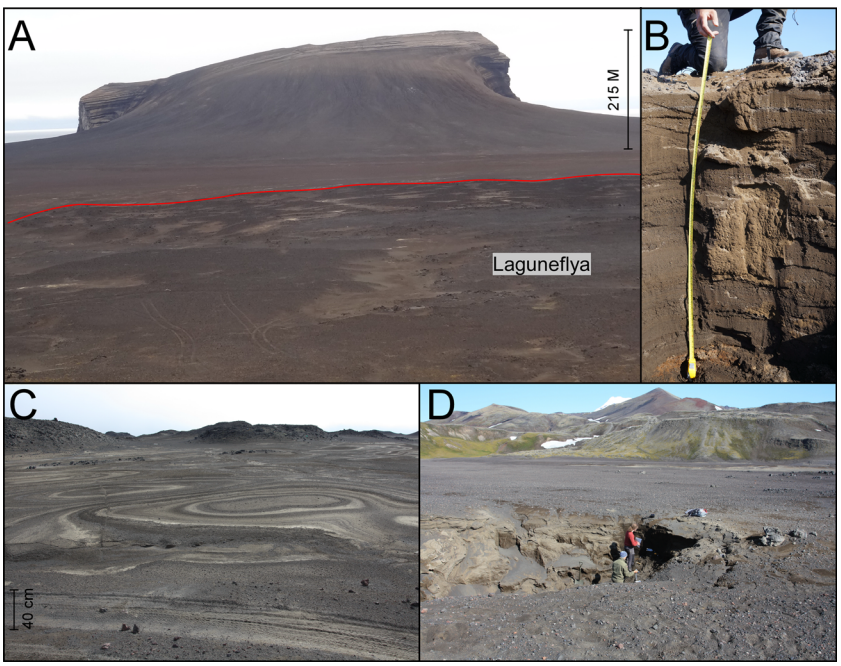

Fig. 3 **a** Eggøya tuff cone (with a height of 215 m) and Laguneflya seen from the North; the lava flow (delimited by the *red line*) is almost completely covered by the Eggøya tephra sheet, see Fig. 1 for picture orientation. **b** Close-up of a section through the tephra sheet (130-cm-long measuring tape) in Laguneflya (P5 in Fig. 6). **c** The tephra sheet deposit in Røysflya, here with concentric rings in the tephra layer as the fallout tephra mantled an Aa-lava flow, subsequent wind erosion has exposed this pattern; wheel tracks in foreground for scale. **d** The tephra sheet deposit and a thermokarst pit in Laguneflya (P5 in Fig. 6), exposing the internal layering of the tephra deposit covering the lava flow; people for scale

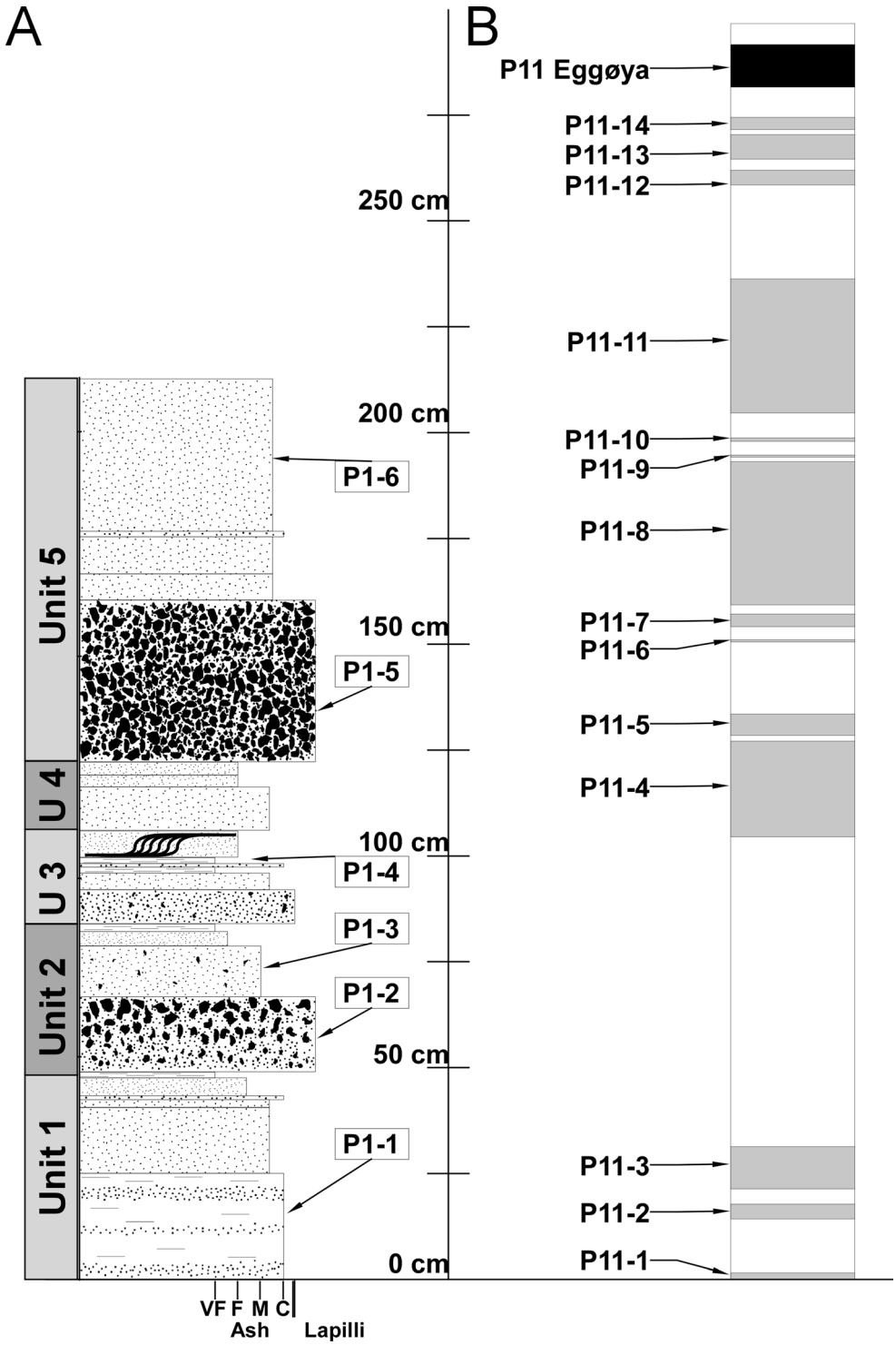

Fig. 4 **a** Stratigraphic column of the P1 section in the Eggøya tephra sheet, divided into five units and showing samples P1-1 to P1-6; note the dune structure in unit 4 and the two coarser grained layers (samples P1-2 and P1-5), each unit is generally characterised by normal grading. **b** Stratigraphic column of the P11 section where Eggøya tephra was found in a soil section together with 14 other tephra layers (for location of the sections, see Fig. 6)

Unit 2 starts with a medium bed (17 cm) consisting of reverse graded lapilli rich in golden pumice (sample P1-2). It is overlain by a medium bed (12 cm) of medium to coarse ash with some lapilli sized grains (sample P1-3). The uppermost part of unit 2 consists of a thin bed (3 cm) of brown fine ash and a very thin bed (2 cm) of gray very fine ash.

Unit 3 starts with a thin bed (8 cm) of coarse ash to fine lapilli, followed by a thin bed (6 cm) of coarse brown ash.

Next follows a lamina (0.5 cm) of very fine gray ash overlain by a lamina (0.5 cm) of coarse black ash. The next deposit is a thin bed (3 cm) of fine to very fine ash (sample P1-4). This bed is overlain by a thin bed (6 cm) showing dune structures and covered by fine ash with ACL.

Unit 4 starts with a medium bed (10 cm) of ash with a medium ash size matrix and some coarse grains beneath a very thin bed (total thickness of 2 cm) of fine ash with a thin cover of very fine ash. This unit is topped with a thin bed (3 cm) of medium ash.

Unit 5 starts with thick bed (37 cm) of clast supported lapilli size tephra that is rich in golden pumice (sample P1-5), followed by a thin bed (6 cm) of coarse to medium ash and a thin bed (8 cm) of coarse ash in a medium ash matrix. The top of this unit consists of a very thin bed (2 cm) of coarse ash followed by a thick bed (35 cm) of a medium ash matrix with some grains of coarse ash (sample P1-6); the last layer is very rich in ACL.

Above Unit 5, we only found reworked tephra with abundant red, oxidised and rounded tephra grains and no apparent structure.

In other sections in the Røysflya and Laguneflya, the tephra layer consists mostly of fine to coarse ash, with occasional lapilli mixed in. The thickness of the deposit in the proximal area ranges from 210 to 37 cm (Fig. 5).

Distal sections

The distal sections of the Eggøya tephra sheet are all made up of grey fine to medium size ash. In mid Sør-Jan at some 22 km distance from the source, we observed the layer down to 1 cm thickness. In Nord-Jan, at some 11 km distance, the tephra layer is 2.5 cm thick. In general, we do observe increasing thickness of the layer towards the Eggøya crater (Fig. 5).

In the sections on the southwest side of Jan Mayen, the tephra is deposited on soils covering Holocene lava flows and beaches (Fig. 5). The tephra layer in these locations is overlain by a thin cover of soil and moss ranging from 1 to 5 cm in thickness.

In the sections to the NW of Eggøya, the ash was deposited on moss and soil covering Holocene and older lava flows on the flanks of Beerenberg (Fig. 5). Some of the Eggøya ash in these sections is covered by up to 10 cm of soil and moss, while in other locations it remains exposed at the surface. A few sections in this area have more than one tephra layer (Fig. 6) and, between the Eggøya tephra and underlying tephra layers, there is 5–10 cm of soil.

An isopach map (Fig. 5) was generated based on the 25 observed sections. As some of the sections are reworked and eroded in the top, this map represents the minimum thickness of the deposit. The thinning half-distance, calculated with the method of Pyle (1989), for a single line segment representing the whole deposit has a value of 0.978 km while when calculated with two line segments (one representing the tuff cone and the most proximal isopach of the tephra sheet and one representing the tephra sheet) gives values of 0.372 km for the proximal segment and 1.678 km for the tephra sheet. This

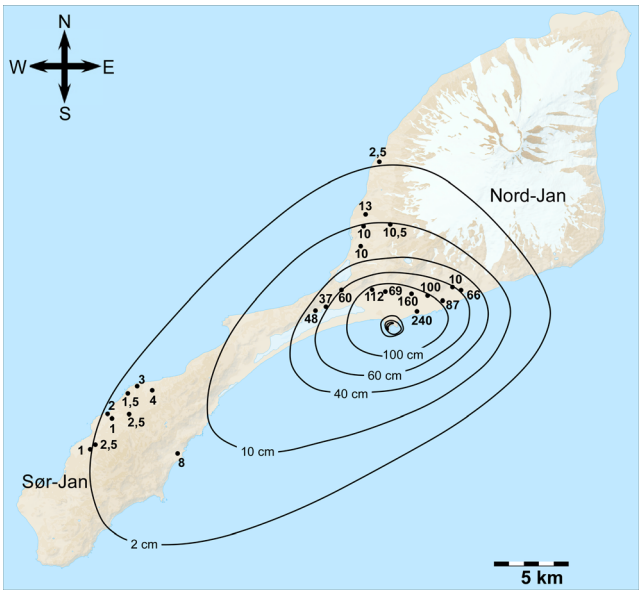

Fig. 5 Isopach map showing the distribution of the 1732 Eggøya tephra. Measured thicknesses for the tephra deposit are shown for each location. All sections are found at low altitudes due to poor preservation and permafrost present at higher altitudes. Base map used with permission, © Norsk Polarinstitutt

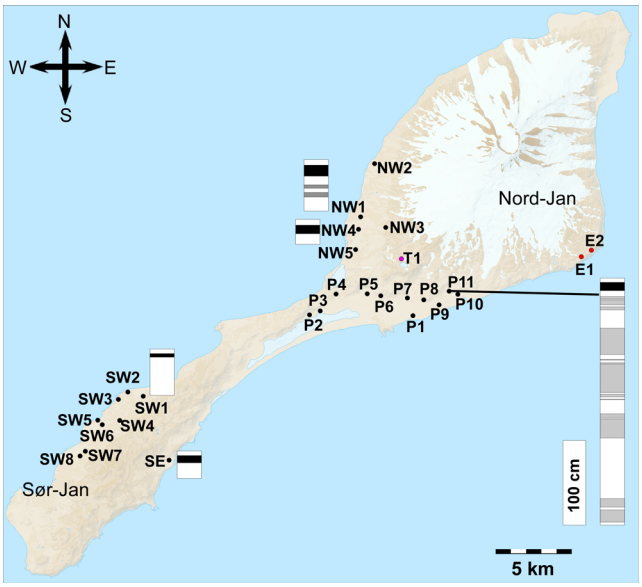

Fig. 6 Map showing the locations of soil sections. Five stratigraphic columns of soil sections are presented; the black layers in the sections indicate the Eggøya tephra sheet. *Black dots* represent where the Eggøya tephra was found; *red* and *purple coloured dots* represent higher altitude sections where the Eggøya tephra was not found, but which contained other tephra layers that were analysed for major element chemistry and reported in Fig. 11. Base map used with permission, © Norsk Polarinstitutt

shows that the deposit is thinning most rapidly in the area from the vent to the 100 cm isopach (2–3.5 km from the vent).

Section P11

About 4 km ENE of Eggøya (Fig. 6), at an altitude of 40 m, we obtained the longest soil section of 2.9 m (Fig. 3b), where a total of 15 tephra layers were observed. The uppermost tephra layer, with a thickness of 10 cm, is the one related to the Eggøya eruption. Eggøya tephra in this section is composed mostly of dark grey medium to coarse ash. It is overlain by 3–5 cm of soil and moss, and separated from the underlying tephra layer by a soil layer of 8–10 cm. The other tephra layers in this section are composed of coarse-grained ash to lapilli and scoria, and are generally much coarser than the Eggøya tephra layer.

Characterisation of tephra sheet deposits

The juvenile fragments of the Eggøya deposit consists of brown sideromelane- and opaque tachylite-glass (Fig. 7a, b), phenocrysts of yellowish to lime green olivine, green to black pyroxene and minor amounts of feldspar. The glass groundmass contains microlites of plagioclase, titanomagnetite and spinel. The ratio of sideromelane to tachylite glass in the 4–3.5 φ (63–90 μm) range is typically around 80 % sideromelane to 20 % tachylite. The sideromelane content decreases with increasing grain size down to 70–75 % in the

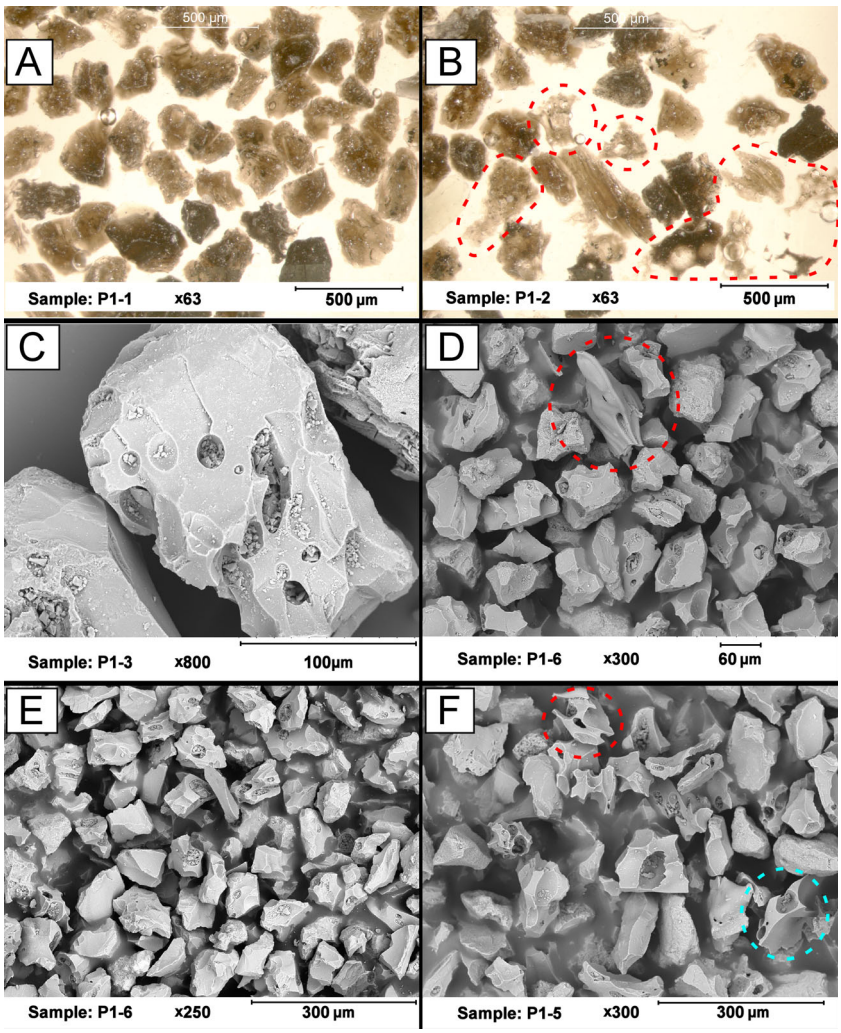

Fig. 7 **a**, **b** Microscope image of polished mounts of tephra from the 2.5 φ (180 μm) size fraction from the P1 section showing the difference in grain morphology between the hydromagmatic phases containing mostly blocky grain shapes (**a**) and more magmatic phases with a higher portion of irregular and vesicular grain shapes (*circled in red*) (**b**). **c** SEM image showing a tephra grain with blocky morphology and smaller tephra grains adhering to vesicles. **d** Mostly blocky tephra shards from the P1-6 sample, with one fluidal shard *circled in red*. **e**, **f** SEM images of tephra grains from the 4 φ (63–90 μm) size fraction (**e**) and 2.5 φ (180 μm) size fraction (**f**), showing typical grain morphology in the more magmatic phases with bubble-wall shards (*circled in blue*) and the more angular irregular shards (*circled in red*)

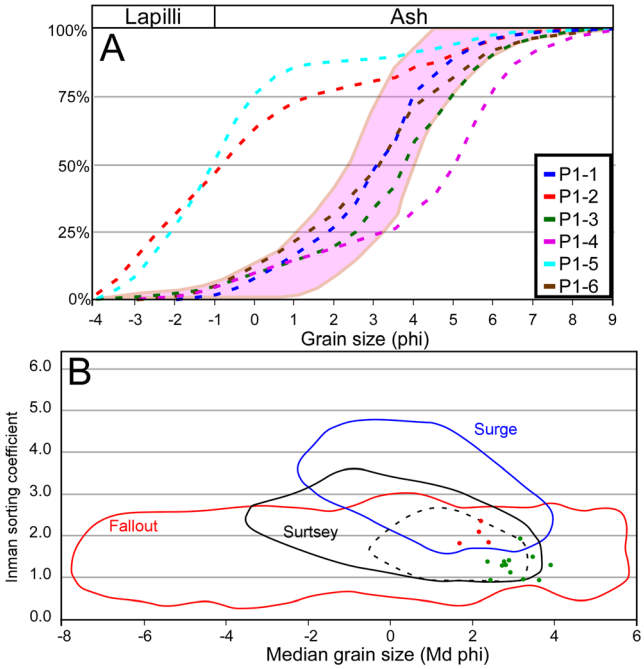

Fig. 8 **a** Cumulative grain size distribution range for the tephra sheet, with *lines* representing samples from internal layering (layers 1–6) from section P1 (Fig. 4a); samples P1-2 and P1-5 have a markedly coarser grain size distribution than the rest of the deposit. **b** Sorting versus median phi of the deposit plotting within the pyroclastic fallout in the diagram of Walker (1971) and showing sorting and median grain sizes very similar to samples collected near the Surtsey vent (*dashed black line*; Walker and Croasdale 1971; the *bold black line* represents samples further away from the Surtsey vent). The proximal (<5 km) samples (*red dots*) are generally coarser and less sorted than the more distal (>5 km) samples (*green dots*)

2.5–2 φ (180–250 μm) size interval, while tachylite makes up 25–30 % and phenocrysts and phenocryst fragments make up around 2 %.

Grain size

The tephra sheet deposit is overall fine grained and poorly to moderately sorted with samples having a median grain size (Mdφ) ranging between 1.5 and 3.5 φ (355–90 μm) and an Inman sorting coefficient (σφ) ranging between 2.3 and 0.95.

Figure 8a shows the ranges of the measured cumulative grain sizes for all Eggøya samples in the coloured area; these samples represent whole sections through the tephra sheet. The dashed lines represent individual samples from the P1 section, and the P1-2 and P1-5 samples show a markedly coarser grain size distribution compared to the rest of the samples both in the P1 section and in the other sections. Figure 8b shows the sorting plotted against median grain size, the more distal (5+ km) tephra sheet deposits are generally finer grained and better sorted (median grain size of 3.91–2.36 φ for the distal deposits) than the proximal ones (1.8–5 km), with sorting ranging from poorly to moderately sorted (sorting coefficient of 1.95–0.95) while the proximal deposits are very poorly to poorly sorted (sorting coefficient 2.36–1.81) and coarser but still fine grained (median grain size of 2.37–1.67 φ).

Individual grain size distributions of samples from proximal, distal NW and distal SW of the crater are presented in Fig. 9 along with the total grain size distribution of the deposits. The grain size is generally coarser in the most proximal samples, but the SW1 and SE samples show coarser grain sizes than the NW distal samples, even though they are further from the vent. The total deposit is polymodal, finely fragmented, with a median grain size (Mdφ) between 2 and 2.5 φ (250–180 μm) and a sorting coefficient of 2.2, with over 80 % of the deposit having a grain size smaller than 0 φ (1 mm).

The sizes of crystal fragments vary within the different phases of the eruption and with distance from the vent. In the P1 section, maximum sizes vary between −1 and −1.5 φ (2000–2800 μm) for pyroxene and olivine, and from 1 to −0.5 φ (500–1400 μm) for feldspar. The biggest crystal fragments are found in the coarsest grained samples (P1-2 and P1-5), while the smallest ones are found in the finer grained ones (P1-3 and P1-4). For the distal samples, crystal fragment sizes also decrease similar to grain size, the coarser SE sample has maximum sizes of between 0 and −0.5 φ (1000–1400 μm) for pyroxene and olivine, and 1 to 0.5 φ (500–710 μm) for feldspar, while the finer SW and NW samples have maximum sizes of 0.5 to 0 φ (710–1000 μm) for pyroxene and olivine, and 1.5 to 1 φ (355–500 μm) for feldspar.

Lithic fragments show the same pattern of variation as the crystal fragment sizes (increasing size towards the vent and increasing size with increasing coarseness of the sample).

Grain morphology

Grains observed with a SEM and a stereo microscope were classified into different morphologies: blocky, fusiform, platy, spherical, irregular, bubble-wall shards and fluidal, based on the grain morphologies described in Cashman et al. (2000), Morrisey et al. (2000) and Dellino et al. (2001). The stereomicroscope studies show that most grains in most samples are blocky (Fig. 7c), with small amounts of other grain shapes (bubble-wall shards and fluidal). Blocky morphologies make up 65–85 % of the P1-1, P1-3, P1-4 and P1-6 (Fig. 7d, e) samples in the 2–2.5 φ size interval (250–180 μm), with small amounts of other grain shapes. Two samples from the P1 section (P1-2 and P1-5) have a much coarser grain size than the other four samples from the same section (Fig. 8a). They also contain a higher abundance of irregular- and bubble-wall-type morphologies; these two morphologies make up around 60 % of grains in P1-2 (Fig. 7b) and around 80 % of the grains in P1-5 (Fig. 7f) [measured in the 2–2.5 φ (250–180 μm) size interval].

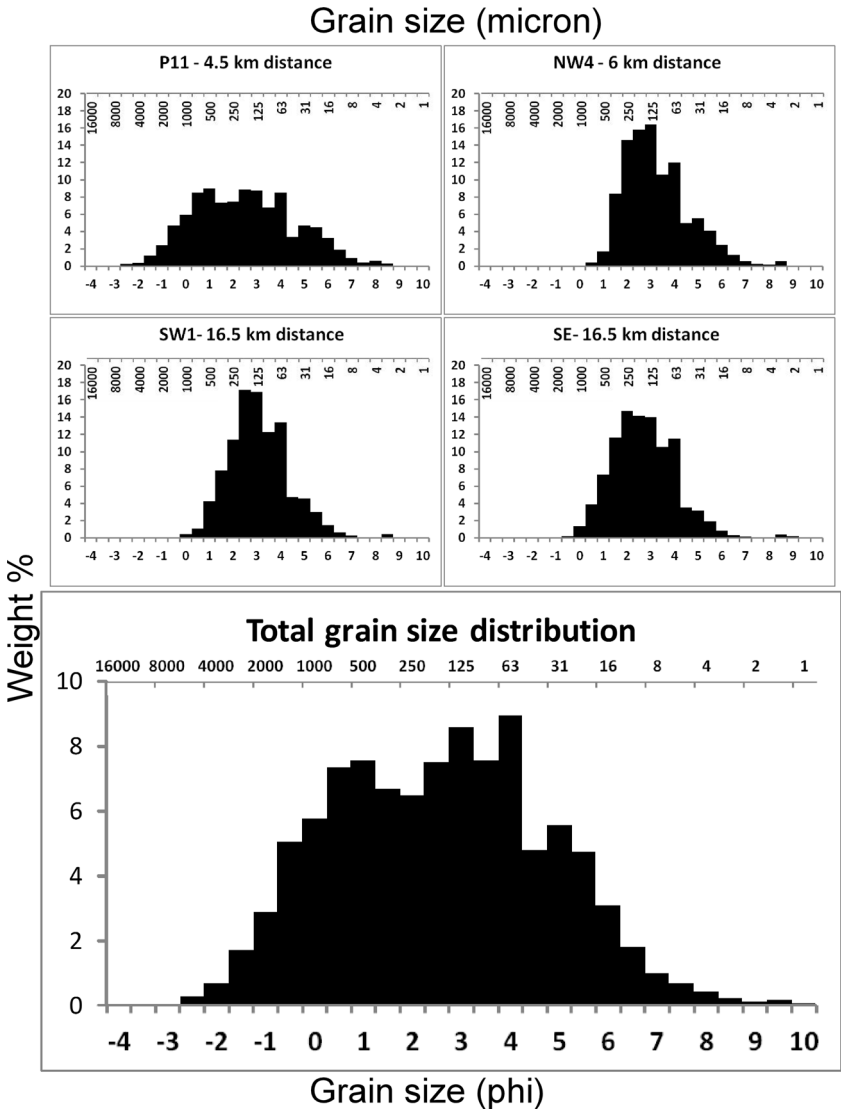

Fig. 9 Grain-size distributions of proximal and distal sections and the total grain-size distribution for the Eggøya tephra sheet calculated using the Matlab script TOTGS of Biass and Bonadonna (2014). The most distal samples (SW1 and SE) have two modes each; NW4 has three modes and, in the P11 section, the Eggøya tephra has four modes

The SEM studies show the same pattern of variation between the samples from the proximal and distal sections; the blocky grains dominate most of the samples, with small amounts of other grain shapes in most samples. The two coarse-grained phases (P1-2 and P1-5) of the proximal section also have a much higher abundance of irregular- and bubble-wall-type morphologies in the SEM studies (Fig. 7b, f). The relative proportion of irregular- and bubble-wall-type morphologies increases with increasing coarseness of the sample.

Volume and mass

The volume of the tephra sheet deposit was calculated using exponential fitting methods. These methods all involve fitting functions to a plot of thickness values versus the square root of the area beneath the associated isopach contour (Fig. 10). We also tried using the inversion technique of Connor and Connor (2006), but this did not yield good results for the Eggøya eruption because it lasted for a long time and changed eruptive style through the eruption.

For the power-law method, the values for this eruption give a coefficient of 2.104. When the power-law coefficient is larger than 2 (for rapidly thinning deposits), the integration of the power-law fit is not very sensitive to the integration limits (Bonadonna and Houghton 2005). For this method, the proximal integration limit was set to 0.43 km^2 (using the method of Bonadonna and Houghton 2005) while the distal limit was varied between 500 and 2000 km^2.

The tephra volumes calculated from these methods are as follows: 0.404 km^3 (Fierstein and Nathenson 1992, two-segment exponential), 0.341 km^3 (Fierstein and Nathenson 1992, three-segment exponential), 0.354±0.029 km^3 (Bonadonna and Houghton 2005, power law) and 0.302 km^3 (Bonadonna and Costa 2012, Weibull method). These determined volumes and a deposit density of 1250 to 1400 kg/m^3 correspond to a total erupted mass range of 4.23–5.66×

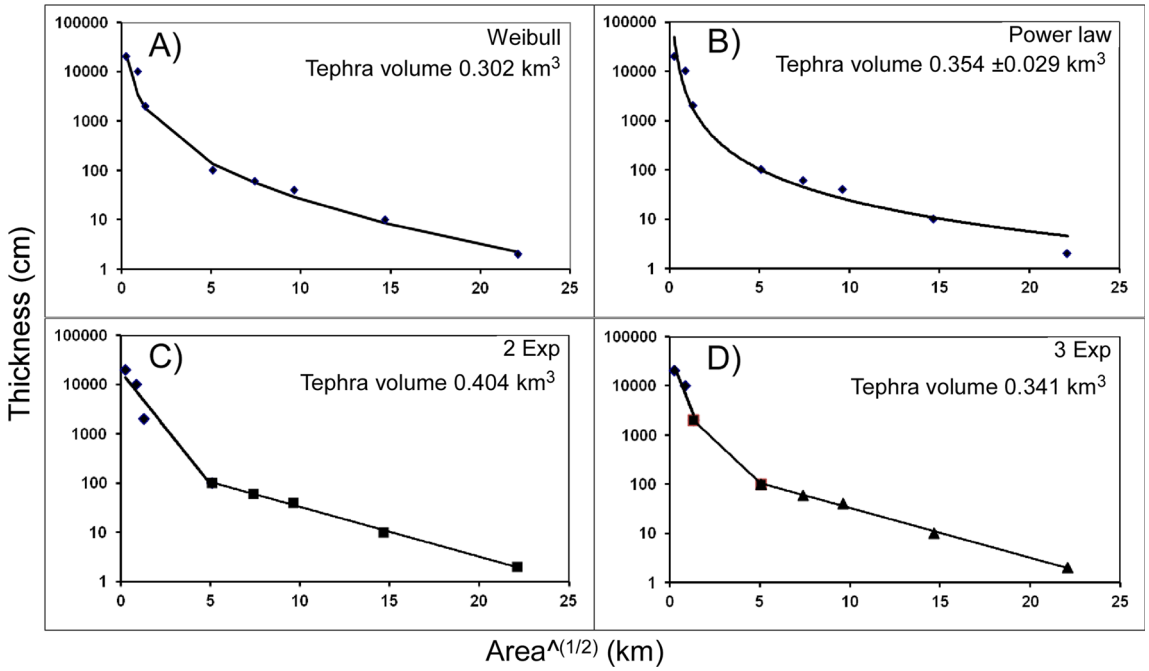

Fig. 10 Volume plots for the Eggøya tephra: Figure (**a**) uses two exponential segments; figure (**b**) uses three exponential segments (Fierstein and Nathenson 1992); figure (**c**) uses the power law of Bonadonna and Houghton (2005); figure (**d**) makes use of the Weibull function by Bonadonna and Costa (2012)

10^{11} kg, and to between 0.16 and 0.21 km^3 of dense rock equivalent (DRE).

Chemical and petrological characteristics

The juvenile fragments of the Eggøya tephra sheet deposit are porphyritic and consist of a microcrystalline glassy groundmass containing microlites of plagioclase, titanomagnetite and spinel together with mineral shards consisting of olivine, pyroxene, plagioclase and oxides in order of decreasing abundance counted in the 2.5–2 φ (180–250 μm) size interval.

The analysed glass shards from the Eggøya eruption mostly plot within the basanite–tephrite compositional field, and presence of olivine crystals define it as basanite, with some samples in the trachybasaltic compositional field of the total alkali versus silica (TAS) diagram of Le Maitre et al. (2002) (Fig. 11a), and all of them plot within the Jan Mayen compositional field (Fig. 11a) of Wallrabe-Adams and Lackschewitz (2003). All the trachybasaltic shards have a Na_2O wt.% that does not exceed the K_2O wt.% by more than 2 wt.% and are, therefore, considered potassic-trachybasalts, and their Si and K values classify them as high K basalts in the classifications of Le Maitre et al. (2002).

The Eggøya samples were also plotted in TiO_2 versus MgO and TiO_2 versus K_2O diagrams (Fig. 11b, c), along with samples from the 1818 eruption (E1 and E2 in Fig. 5) found on the SE slopes of Beerenberg, one other eruption from section T1, other Jan Mayen eruptions from section P11 and a bulk analysis of the 1970 eruption (Siggerud 1972; Weigand 1972). The analysed Jan Mayen eruptions mostly plot within the basanite/tephrite to trachybasaltic fields (Fig. 11a), with a few eruptions overlapping into the basalt, phono-tephrite and basaltic trachy-andesite fields.

Discussion

Age of Eggøya

Imsland (1978) estimated the Eggøya tuff cone to be a young structure with volcanic activity having occurred a few hundred years ago. However, the deposits have not been precisely dated.

The historical descriptions of the 1732 eruption mention an ash cloud and incandescence, along with thick ash deposits covering large parts of the island and reaching distances of at least 111 km (15 German miles) away into the sea, thus indicating an explosive eruption. However, the previously assigned eruption sites for the 1732 eruption are craters with effusive activity (Scoresby 1820; Wordie 1922; Imsland 1978), and the Røysflya and Laguneflya Holocene lava flows (Fig. 1c) previously proposed to have originated from the 1732 and 1818 eruptions (Imsland 1978) are covered by the extensive tephra sheet originating from Eggøya. The deposits on these lava flows have numerous thermokarst depressions (Fig. 3d) indicating that the tephra was at least partly deposited on snow and, together with the preservation of the primary

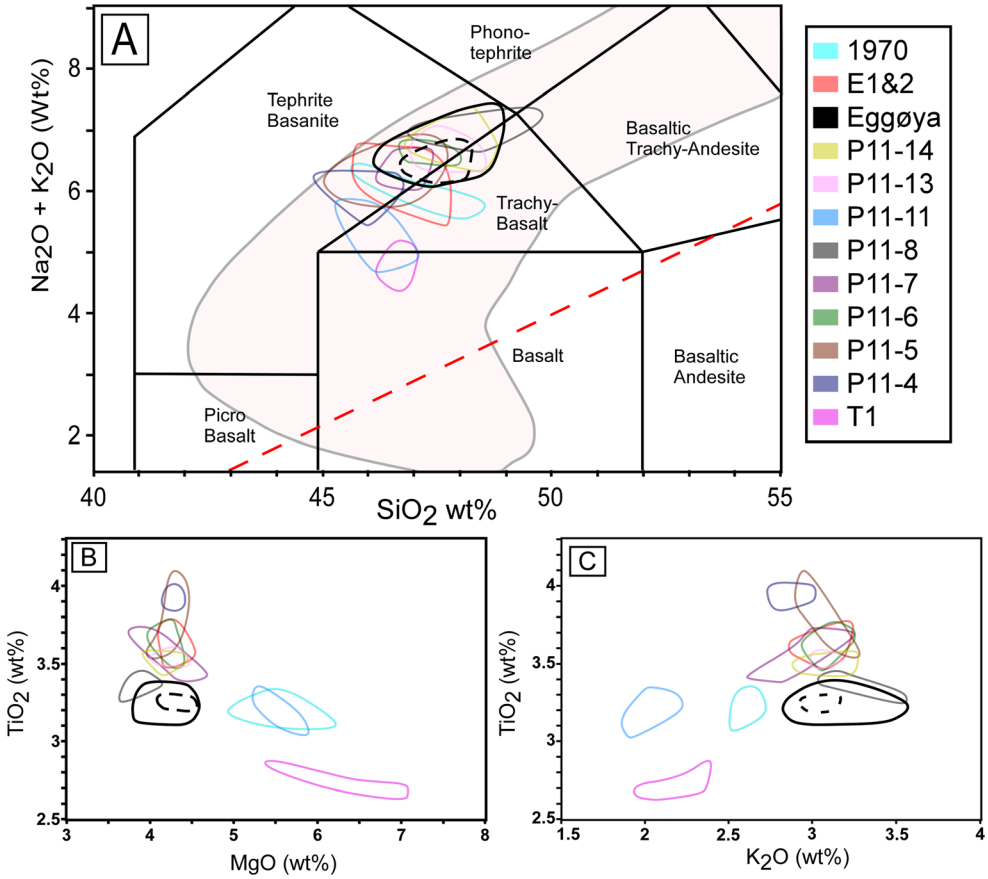

Fig. 11 Chemistry of Jan Mayen tephras, showing compositions of Eggøya tephra sheet along with other tephra layers sampled on the island, using eight tephra layers from section P11 that were suitable for chemical analysis, using tephra collected in sections T1, E1 and E2 (Fig. 4). Bulk analysis of the 1970 eruption by Siggerud (1972) and Weigand (1972) is also presented. Tephra from the sediment core (*dashed black line*) plots directly within the Eggøya composition field. **a** Total alkali versus silica shows that the Eggøya tephra spans the field of trachybasalt to basanite–tephrite; the *shaded field* represents the Jan Mayen compositional field from Wallrabe-Adams and Lackschewitz (2003). **b** TiO_2 versus MgO shows that the Eggøya tephra is compositionally separated from other layers, although there is an overlap with an older tephra, P11-8. **c** TiO_2 versus K_2O, also separates the Eggøya tephra from other layers but still there is an overlap with P11-8

tephra layer mostly at altitudes lower than 100 m, is consistent with an eruption during spring when only the lower altitudes are relatively snow-free but still with patches of snow in depressions.

Maps from 1664 to 1702–1720 show a small island named 'Eyjereyland', 'Rocher des Oiseaux' or 'Vogel clippen' not far from present-day Eggøya, but the coastline was located behind this island and the Sørlaguna lagoon is not present. The first map showing the Eggøya tuff cone and Sørlaguna is from 1769 and shows the tuff cone attached to the mainland and located between 'Eyjereyland' and Jan Mayen. Maps after 1877 do not show 'Eyjereyland' indicating that the island had been fully eroded by the sea.

A cryptotephra horizon in the GS11-169-16GC sediment core (Fig. 1a), containing glass with geochemistry similar to that of the Eggøya tephra (see Fig. 11), occurs with a maximum concentration 1–1.5 cm from the top of the core. The age model for this core (Gjerløw et al., in preparation) with a sedimentation rate of 200 to 340 years/cm gives this horizon an age range overlapping with the 1732 eruption.

The deposits from Eggøya (tuff cone and tephra sheet) fit well with the historical descriptions of the 1732 eruption, and the time of year fits well with the distribution and structures seen in the deposits. The isopachs of the tephra sheet are centred around the Eggøya tuff cone; it is the youngest tephra layer found in soil sections and it remains vegetation free in large areas. Further, steam and warm air are still coming from cracks along the crater rim of Eggøya, attesting to a young age. This leads us to believe that Eggøya must be the source of the 1732 eruption of Jan Mayen.

Grain morphology

Most of the studied samples from the proximal, medial and distal tephra sheet show mostly blocky, equant grain shapes with stepped fracture surfaces, and smaller particles adhering

to glass surfaces and vesicles are common (Fig. 7a, c, d, e). These types of grain shapes and features are commonly found in deposits of Surtseyan eruptions like Surtsey (Wohletz 1983), Black Point (Murtagh and White 2013) and Ilchulbong (Sohn and Chough 1992; Murtagh et al. 2011). They are interpreted to indicate magma–water interaction causing brittle fragmentation as a result of rapid quenching of magma and thermohydraulic explosions (Büttner et al. 1999; Morrisey et al. 2000; Dellino et al. 2001). The ash also contains small amounts of grains with morphologies that are associated with magmatic fragmentation (bubble wall, fluidal and irregular morphologies).

In the P1 section (Fig. 4a), the P1-2 and P1-5 samples have coarser grain sizes than the other samples. These samples also show different grain morphology compared to the other samples in the section, with 60–80 % of irregular, bubble wall shards and fluidal morphologies (Fig. 7b, f). These morphologies are associated with a magmatic fragmentation mechanism, driven by the exsolution and expansion of gasses dissolved in the magma (Cashman et al. 2000; Morrisey et al. 2000; Dellino et al. 2001). They also contain smaller amounts of grains with blocky morphology commonly associated with hydromagmatic fragmentation.

This indicates changing eruptive conditions during the course of the eruption, most likely through changing water to magma ratios, influenced either by the ease of sea water accessing the vent or by changing eruption rates, similar to Surtsey and Capelinhos where marine erosion and explosive activity at times breached the walls of the cones allowing easy access of sea water to the vent, while at other times the vent was partly shielded by walls of tephra (Thorarinsson et al. 1964; Cole et al. 2001). Deposits of the two phases with more magmatic grain morphologies are only found in the P1 section. In the distal section, the grain shapes are mostly consistent with hydromagmatic fragmentation, indicating that the tephra produced by the more magmatic phases had a much more limited dispersal than that of the hydromagmatic phases.

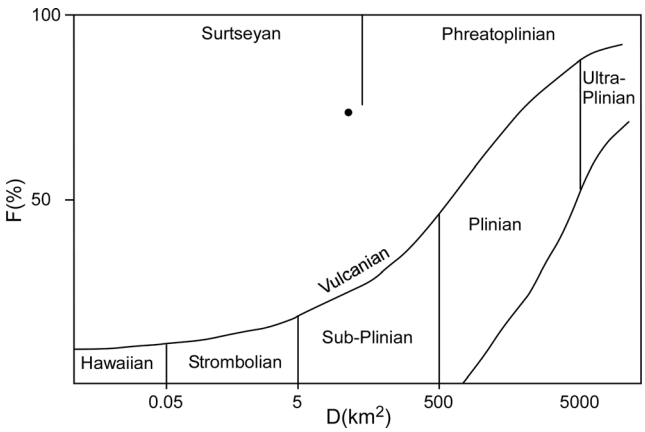

Fig. 12 The Eggøya tephra sheet plotted on a diagram of fragmentation (F, %) versus dispersal (D, km^2), from Walker (1973). The Eggøya eruption plots within the Surtseyan field

Eruption rate, style and interpretation of deposit

Based on the historical accounts of the eruption, it lasted for a minimum of 4 days and up to a maximum of around 40 days. This gives an average mass discharge rate for the deposit ranging between 1.22 and 1.64×10^6 kg/s for a 4-day eruption and 1.22–1.64×10^5 kg/s for a 40-day eruption with the calculated mass ranges.

In the F/D plot of Walker (1973) (Fig. 12), where D equals the dispersal of the $0.01\times T_{max}$ isopach (200 cm in this case) extending for 26 km^2, and F equals the portion of deposit finer than 1 mm at the $0.1\times T_{max}$ along the main dispersal axis (73 % for our section closest to this point), the Eggøya tephra sheet fits into the Surtseyan domain.

The Eggøya tuff cone has an aspect ratio of 0.33, similar to tuff cones found in Iceland and Hawaii (Wohletz and Sheridan 1983), and appears similar in shape. The eruption was dominated by fallout deposition, similar to other tuff cones. In observed emergent Surtseyan eruptions like the eruptions of Surtsey (Thorarinsson et al. 1964) and Capelinhos (Cole et al. 2001), three main types of activity have been observed: tephra jets, most common when seawater had easy access to the vents; continuous uprush, most common when the vents were surrounded by walls of tephra leading to more efficient heat exchange (Kokelaar 1986); and lava fountaining when the vents were surrounded by walls of tephra and built up to a higher level than the sea surface, effectively cutting off sea water access. Tuff cones are formed mainly by fallout deposits from tephra jets at higher proportions of water, and continuous uprush when more efficient heat exchange occurs (Sheridan and Wohletz 1981; Wohletz and Sheridan 1983; Kokelaar 1986; White and Houghton 2000).

The columns associated with continuous uprush in Surtsey and Capelinhos were seen to contain a significant portion of incandescent material and were seen reaching heights of up to at least 9000 m in the case of Surtsey (Thorarinsson et al. 1964; Sigurgeirsson 1965; Kokelaar 1983; Cole et al. 2001). The tephra jets, especially the more powerful and oblique ones, caused surges moving down the slopes or through openings in the crater walls, sometimes reaching hundreds of metres over the sea (Thorarinsson et al. 1964).

The grain morphology and features of most samples from the Eggøya tephra sheet are indicative of hydromagmatic fragmentation (Morrisey et al. 2000; Dellino et al. 2001). Further, the ductile deformation structures formed by the impact of ballistic fragments and syn-eruptional slumping in the cone (Fig. 2a, b) and the generally fine grain size of the Eggøya deposits (cone and sheet) is consistent with a Surtseyan eruption with a mainly wet hydromagmatic eruption style caused by the interaction of sea water and magma, similar to what is

seen in wet hydromagmatic facies from other tuff cones and hydromagmatic eruptions (Cole et al. 2001; Solgevik et al. 2007; Murtagh et al. 2011; Pedrazzi et al. 2013; Van Otterloo et al. 20133). Abundant dunes (Fig. 2c) seen in the flanks of the Eggøya tuff cone also indicate numerous surges that are common in hydrovolcanic eruptions (Wohletz and Sheridan 1983; Fisher and Schmincke 1984; Walker 1984). We also interpret dune structures found in the most proximal profile P1 of the Eggøya tephra sheet (Fig. 3a) to have formed due to surges, indicating that they reached a distance of at least 1.8 km from the vent, similar to Capelinhos where some surges reached distances of a least 2 km (Cole et al. 2001).

Eruption scenario

Maps predating the eruption show that the present location of Eggøya was open water prior to the eruption. This suggests that the eruption started out as a shallow submarine eruption that gradually built an edifice reaching out of the sea similar to other Surtseyan eruptions. There may be an ash platform under the tuff cone like that seen at Pahvant Butte (White 1996). The Eggøya eruption was wet throughout the activity, but the deposits suggest that the ratio of magma to water mixing changed back and forth during the eruption, possible reasons being changing eruption rates or changes in water access to the vent. At Surtsey and Capelinhos, it was seen that at times the eruptions built walls surrounding the vent and limited water access, while at other times exposed areas of the cones would be eroded by waves and explosions and increase water access to the vent (Thorarinsson et al. 1964; Cole et al. 2001). We interpret the interplay between erosion, in the form of waves and explosions, and construction of the cone by deposition of tephra as the main cause of changing water/magma ratio in this eruption.

Similar to Surtsey and Capelinhos, we suggest three main types of activity: tephra jets, continuous uprush and more magmatic phases. During periods when sea water had easy access to the vent, tephra jets produced numerous surges and are responsible for the abundant surge deposits seen in the flanks of the tuff cone; during periods with less sea water access, continuous uprush produced the main fallout deposits in the tephra sheet and the tuff cone, and finally the driest phases produced the coarser grained and more magmatic morphologies found in the proximal deposits in the cone and sheet.

Contemporaneous observation indicated that at the time of the highest effusion, incandescent (temperature above 650 °C) material was ejected, suggesting dryer conditions. There is no evidence of lava formation in the eruption, indicating that water was supplied to the vent in various degrees throughout the eruption. Tephra fell at least up to 111 km away from the island of Jan Mayen. This suggests that the eruption plumes could have been similar to what was observed in Surtsey with heights of up to 9–12 km (Sigurgeirsson 1965).

Volume determination

There is a good agreement in the volumes calculated using the different methods, with a spread from 0.302 to 0.404 km^3. Present-day wind data from the NCEP-DOE AMIP-II Reanalysis database (Kanamitsu et al. 2002) shows that winds at 5 and 10 km height in the area generally blow to the east. Parts of the tephra were deposited at sea and, due to difficult coring conditions, we were unable to obtain thickness data proximal to Jan Mayen. This lack of thickness data in the sea around Jan Mayen, especially in the sea south and east of Eggøya (where the present-day winds are more likely to blow tephra), makes the isopach map uncertain. Due to this uncertainty, the volume calculation is at a minimum. Nevertheless, our calculated volume of Eggøya and the tephra sheet (0.16–0.21 km^3 DRE), when compared to the average volume (0.071 km^3) for Holocene eruptions on Jan Mayen by Imsland (1978), is two to three times higher. It is smaller than the volume of the 1970 eruption that produced at least 0.5 km^3 of lava (Siggerud 1972) and larger than the 1985 eruption that produced around 0.007 km^3 of lava (Imsland 1986). The estimated ranges of tephra volume for this eruption fall within magnitude 4 of the Volcanic Explosivity Index (VEI) of Newhall and Self (1982) and a hypothetical plume height similar to Surtsey (9–12 km) places the eruption in the VEI 3–4 category. Previously described eruptions of Jan Mayen were much less explosive, with the 1970 eruption producing around 0.025 km^3 (DRE) of tephra similar to a VEI 2 eruption, but only in the early phases of the eruption, when melt water from the glaciers flowed into the craters, was there any stratospheric injection (Siggerud 1972).

Geochemistry

The chemical composition of the Eggøya tephra in the P1 section has the same composition throughout the deposit (Table 1) and is similar to the other analysed samples from Jan Mayen (Fig. 11). This could indicate that little or no differentiation of the magma occurred prior to the eruption. The eruptive style of Surtseyan volcanism does, however, lead to extensive recycling of previously erupted material (Kokelaar 1983). This could affect the measured chemistry in the later samples. Similar to Black Point (Murtagh and White 2013), we see an increase in the amount of tachylite with increasing grain size. The more crystalline texture of the tachylite could thus be a result of slower cooling within larger tephra grains, while the glassy texture of the sideromelane is formed by rapid cooling of the erupting magma.

The major element chemistry of the 1732 eruption falls mostly within the tephrite–basanite field, similar to tephra

from other Beerenberg flank eruptions in the P11, T1, E1 and E2 sections (Fig. 11a), and the presence of olivine define it as basanite. The other chemical plots (Fig. 11b, c) show that it is possible to distinguish the Eggøya tephra from the other eruptions, with Eggøya showing higher ranges of K_2O than most of the other eruptions. Tephra from the cryptotephra horizon close to the top of the sediment core SW of Jan Mayen plots directly within the ranges of only the Eggøya eruption in all the different plots, suggesting that it originates from this eruption.

Conclusions

The Eggøya tuff cone and its deposits on Jan Mayen were produced during a Surtseyan emergent eruption that breached the sea surface on the 17th of May 1732 and lasted 4 to 40 days. It produced an estimated bulk tephra volume of at least 0.3–0.4 km^3, equivalent to 0.16–0.21 km^3 DRE over the course of the eruption, and corresponds to a VEI 4 eruption, the largest explosive eruption described so far from Jan Mayen. The stratigraphy of the deposits and maps made before 1732 suggests that the eruption started out as a shallow submarine eruption that gradually emerged and built the tuff cone, shifting between three main types of activity during the eruption, dependent on water access to the vent and the efficiency of the heat exchange between the water and magma: wet tephra jets producing surges and associated deposits along with some amount of fallout deposits, continuous uprush producing the main fallout deposits in the tephra sheet and the tuff cone, and more magmatic phases producing the coarse-grained proximal deposits in the cone and sheet. The tephra sheet deposits covered much of the island of Jan Mayen, and a total area of at least around 500 km^2 is within the 2-cm isopach line. The chemistry of the volcanic glass from this eruption ranges from tephrite–basanite to trachybasaltic composition in the TAS diagram of Le Maitre et al. (2002); it is further classified as a basanite to trachybasalt based on the presence of olivine. It is also classified as high potassium basalts and potassic-trachybasalts according to other classification schemes.

This study has implications for future work assessing volcanic hazards and mitigating measures on Jan Mayen and shows that tephra fall from Surtseyan eruptions can affect large parts of the island and should be part of future hazard assessments and eruptive scenarios for Jan Mayen.

Acknowledgements This study was part of E. Gjerløw's Ph.D. project and was financed by the Centre for Geobiology at the University of Bergen and the Nordic Volcanological Center at the University of Iceland. We want to acknowledge the Jan Mayen personnel for their hospitality and assistance during fieldwork, Chris Hayward for assistance with microprobing and the Norwegian Polar Institute for supplying aerial photos and map data. Thanks are given to associate editor P.-S. Ross and reviewers Y.K. Sohn and D. Pedrazzi whose comments helped to improve this paper.

References

Anderson J (1746) Nachrichten von Island, Grönland und der Strasse Davis. Hamburg

Barr S (2003) Jan Mayen Norges utpost i vest, Øyas historie gjennom 1500 år. Schibsted forlag, Oslo

Belousov A, Belousova M (2001) Eruptive processes, effects and deposits of the 1996 and the ancient basaltic phreatomagmatic eruptions in Karymskoye lake, Kamchatka, Russia. In: White JDL, Riggs NR (eds) Volcaniclastic sedimentation in lacustrine settings. pp 35–60

Biass S, Bonadonna C (2014) TOTGS: total grainsize distribution of tephra fallout. https://vhub.org/resources/3297

Blaeu J (1650) Insvlæ Jan Mayanæ, Descriptio (map ca. 1:120 000)

Blott SJ, Pye K (2001) GRADISTAT: a grain size distribution and statistics package for the analysis of unconsolidated sediments. Earth Surf Process Landf 26:1237–1248

Boldva AB von (1886) Jan Mayen nach der Aufnahme der Östereich. arc. Beobachtungsstation (Map 1:100 000)

Bonadonna C, Costa A (2012) Estimating the volume of tephra deposits: a new simple strategy. Geologija 40:415–418. doi:10.1130/G32769.1

Bonadonna C, Houghton BF (2005) Total grain-size distribution of tephra-fall deposits. Bull Volcanol 62:493–518. doi:10.1007/s00445-004-0386-2

Büttner R, Dellino P, Zimanowski B (1999) Identifying magma–water interaction from the surface features of ash particles. Nature 401:688–690

Carstens H (1962) Lavas on the southern part of Jan Mayen. Nor Polarinst Åarb 1961:69–82

Cas RAF, Wright JV (1987) Volcanic successions modern and ancient—a geological approach to processes, products and successions. Allen & Unwin, London, 487 pp

Cashman KV, Sturtevant B, Papale P, Navon O (2000) Magmatic fragmentation. In: Sigurdsson H, Houghton BF, McNutt SR, Rymer H, Stix J (eds) Encyclopedia of volcanoes. Academic, New York, pp 421–430

Cole PD, Guest J, Duncan A, Pacheco J (2001) Capelinhos 1957–1958, Faial, Azores: deposits formed by an emergent Surtseyan eruption. Bull Volcanol 63:204–220

Connor LJ, Connor CB (2006) Inversion is the source to dispersion: understanding eruption dynamics by inverting tephra. In: Mader HM, Coles SG, Connor CB, Connor LJ (eds) Statistics in Volcanology, Special Publ of IAVCEI 1. Geological Society, London, pp 231–242. doi:10.1016/j.jvolgeores.2010.03.011

Cox A (1969) Geomagnetic reversals. Science 163:237–245

Cromwell G, Tauxe L, Staudigel H, Constable CG, Koppers AAP, Pedersen RB (2013) In search of long-term hemispheric asymmetry in the geomagnetic field: results from high northern latitudes. Geochem Geophys Geosyst 14:3234–3249. doi:10.1002/ggge.20174

Dellino P, Isaia R, La Volpe L, Orsi G (2001) Statistical analysis of textural data from complex pyroclastic sequences: implications for fragmentation processes of the Agnano-Monte Spina Tephra (4.1 ka), Phlegraean Fields, southern Italy. Bull Volcanol 63:443–461

Fierstein J, Nathenson M (1992) Another look at the calculation of fallout tephra volumes. Bull Volcanol 54:156–167. doi:10.1007/BF00278005

Fisher RV, Schmincke HU (1984) Pyroclastic rocks. Springer, Berlin, p 474

Fitch FJ (1964) The development of the Beerenberg volcanoe, Jan Mayen. Proc Geol Assoc 75:133–165

Fitch FJ, Nairn AEM, Talbot CJ (1965) Paleomagnetic studies on rocks from North Jan Mayen. Nor Polarinst Åarb 1963:49–60

Haase KM, Devey CW, Mertz DF, Stoffers P, Garbe-Schonberg D (1996) Geochemistry of lavas from Mohns Ridge, Norwegian-Greenland sea: implications for melting conditions and magma sources near Jan Mayen. Contrib Mineral Petrol 123:223–237

Hawkins TRW, Roberts B (1972) The petrology of the volcanic and intrusive rocks of Nord-Jan, Jan Mayen. Nor Polarinst Åarb 1970: 19–41

Hayward C (2012) High spatial resolution electron probe microanalysis of tephras and melt inclusions without beam-induced chemical modification. The Holocene 22(1):119–125. doi:10.1177/0959683611409777

Imsland P (1978) The geology of the volcanic island Jan Mayen, Arctic Ocean. Nord Volcanol Inst Res Rep 7813

Imsland P (1984) Petrology, mineralogy and evolution of the Jan Mayen magma system. Visindafelag islendinga, Rit 43, Reykjavik, 332 pp

Imsland P (1986) The volcanic eruption on Jan Mayen, January 1985: interaction between a volcanic island and a fracture zone. J Volcanol Geotherm Res 28:45–53. doi:10.1016/0377-0273(86)90004-1

Kanamitsu M, Ebisuzaki W, Woollen J, Yang S-K, Hnilo JJ, Fiorino M, Potter GL (2002) NCEP-DOE AMIP-II reanalysis (R-2). Bull Am Meteorol Soc 1631–1643

King A, Jennings JN (1939) The imperial college expedition to Jan Mayen island. Geogr J 94:115–131

Kokelaar BP (1983) The mechanism of Surtseyan volcanism. J Geol Soc (Lond) 140:939–944. doi:10.1144/gsjgs.140.6.0939

Kokelaar BP (1986) Magma–water interactions in subaqueous and emergent basaltic volcanism. Bull Volcanol 48:275–289

Le Maitre RW, Streckeisen A, Zanetti B, Le Bas MJ, Bonin B, Bateman P, Bellieni G, Dudek A, Efremova S, Keller J, Lameyre J, Sabine PA, Schmid R, Sørensen H, Woolley AR (2002) Igneous rocks a classification and glossary of terms, 2nd edn. Cambridge University Press, Cambridge

Matsson HB, Höskuldsson A (2011) Contemporaneous phreatomagmatic and effusive activity along the Hverfjall eruptive fissure, north Iceland: eruption chronology and resulting deposits. J Volcanol Geotherm Res 201:241–252

Mattsson HB (2010) Textural variation in juvenile pyroclasts from an emergent, Surtseyan-type, volcanic eruption: the Capelas tuff cone, Sao Miguel (Azores). J Volcanol Geotherm Res 189:81–91

Mohn H, Wille C (1877) Map of Jan Mayen 1:200,000

Morrisey M, Zimanowski B, Wohletz K, Buettner R (2000) Phreatomagmatic fragmentation. In: Sigurdsson H, Houghton BF, McNutt SR, Rymer H, Stix J (eds) Encyclopedia of volcanoes. Academic, New York, pp 431–445

Murtagh RM, White JDL (2013) Pyroclast characteristics of a subaqueous to emergent Surtseyan eruption, Black Point volcano, California. J Volcanol Geotherm Res 267:75–91

Murtagh RM, White JDL, Sohn YK (2011) Pyroclast textures of the Ilchulbong 'wet' tuff cone, Jeju Island, South Korea. J Volcanol Geotherm Res 201:385–396

Newhall C, Self S (1982) The volcanic explosivity index (VEI) an estimate of explosive magnitude for historical volcanism. J Geophys Res 87:1231–1238

Pedrazzi D, Marti J, Geyer A (2013) Stratigraphy, sedimentology and eruptive mechanisms in the tuff cone of El Golfo (Lanzarote, Canary Islands). Bull Volcanol 75:1–17

Pyle D (1989) The thickness, volume, and grainsize of tephra fall deposits. Bull Volcanol 51:1–15. doi:10.1007/BF01086757

Scoresby W Jr (1820) An account of the Arctic regions, with a history and description of the Northern whale-fishery. A Constable & Co, Edinburgh

Sheridan MF, Wohletz KH (1981) Hydrovolcanic explosions: the systematics of water–pyroclast equilibration. Sci New Ser 212:1387–1389. doi:10.1126/science.212.4501.1387

Siggerud T (1972) The volcanic eruption on Jan Mayen 1970. Nor Polarinst Åarb 1970:5–18

Sigurgeirsson T (1965) Some geophysical measurements and observations in Surtsey 1963–1964. Surtsey Res Prog Rep

Sohn YK (1996) Hydrovolcanic processes forming basaltic tuff rings and cones on Cheju Island, Korea. Geol Soc Am Bull 108:1199–1211. doi:10.1130/0016-7606(1996)108<1199:HPFBTR>2.3.CO;2

Sohn YK, Chough SK (1989) Depositional processes of the Suwolbong tuff ring, Cheju Island (Korea). Sedimentology 36:837–855

Sohn YK, Chough SK (1992) The Ilchulbong tuff cone, Cheju Island, South Korea: depositional processes and evolution of an emergent, Surtseyan-type tuff cone. Sedimentology 39:523–544

Solgevik H, Matsson HB, Hermelin O (2007) Growth of an emergent tuff cone: fragmentation and depositional processes recorded in the Capelas tuff cone, São Miguel, Azores. J Volcanol Geotherm Res 159:246–266. doi:10.1016/j.jvolgeores.2006.06.020

Sylvester AG (1975) History and surveillance of volcanic activity on Jan Mayen island. Bull Volcanol 39–2:1–23

Thorarinsson S, Einarsson T, Sigvaldason G, Elisson G (1964) The submarine eruption off the Vestmann Islands 1963–1964, a preliminary report. Bull Volcanol 27:435–445

Trønnes RG, Planke S, Sundvoll B, Imsland P (1999) Recent volcanic rocks from Jan Mayen: low-degree melt fractions of enriched northeast Atlantic mantle. J Geophys Res 104:7153–7716

Tyrrell GW (1926) The petrology of Jan Mayen. Trans R Soc Edinb 54: 747–765. doi:10.1017/S0080456800016161

Van Otterloo J, Cas RAF, Sheard MJ (2013) Eruption processes and deposit characteristics at the monogenetic Mt. Gambier Volcanic Complex, SE Australia: implications for alternating magmatic and phreatomagmatic activity. Bull Volcanol 75:737. doi:10.1007/s00445-013-0737-y

Vespermann D, Schmincke H (2000) Scoria cones and tuff rings. In: Sigurdsson H, Houghton BF, McNutt SR, Rymer H, Stix J (eds) Encyclopedia of volcanoes. Academic, New York, pp 683–194

Walker GPL (1971) Grain size characteristics of pyroclastic deposits. J Geol 79:696–714

Walker GPL (1973) Explosive volcanic eruptions—a new classification scheme. Geol Rundsch 62:431–446

Walker GPL (1984) Characteristics of dune-bedded pyroclastic surge bedsets. J Volcanol Geotherm Res 20:281–296

Walker GPL, Croasdale R (1971) Characteristics of some basaltic pyroclastics. Bull Volcanol 35:303–317

Wallrabe-Adams HJ, Lackschewitz KS (2003) Chemical composition, distribution, and origin of silicic volcanic ash layers in the Greenland–Iceland–Norwegian sea: explosive volcanism from 10 to 300 ka as recorded in deep-sea sediments. Mar Geol 193(3): 273–293. doi:10.1016/S0025-3227(02)00661-8

Weigand (1972) Bulk-rock and mineral chemistry of Recent Jan Mayen basalts. Nor Polarinst Åarb 1970:42–52

White JDL (1996) Pre-emergent construction of a lacustrine basaltic volcano, Pahvant Butte, Utah. Bull Volcanol 58:249–262

White JDL, Houghton B (2000) Surtseyan and related phreatomagmatic eruptions. In: Sigurdsson H, Houghton BF, McNutt SR, Rymer H, Stix J (eds) Encyclopedia of volcanoes. Academic, New York, pp 495–511

Wohletz KH (1983) Mechanisms of hydrovolcanic pyroclast formation: grain size, scanning electron microscopy and experimental studies. J Volcanol Geotherm Res 17:31–63

Wohletz KH, Sheridan MF (1983) Hydrovolcanic explosions; II, evolution of basaltic tuff rings and tuff cones. Am J Sci 283:385–413
Wordie JM (1922) Jan Mayen island. Geogr J 1922:180–194
Wordie JM (1926) The geology of Jan Mayen. Trans R Soc Edinb 54: 741–745
Zanon V, Pacheco J, Pimentel A (2009) Growth and evolution of an emergent tuff cone: considerations from structural geology, geomorphology and facies analysis of Sao Roque volcano, Sao Miguel (Azores). J Volcanol Geotherm Res 180:277–291